MHD FLOW IN A RECTANGULAR CHANNEL WITH APPLICATION TO A MARINE PROPULSION SYSTEM USING SUPERCONDUCTING MAGNETS

by

LIEUTENANT ROBERT A. DORAGH, U.S.N.

SUBMITTED IN PARTIAL FULFILLMENT
OF THE REQUIREMENTS FOR THE
DEGREE OF NAVAL ENGINEER
AND THE DEGREE OF
MASTER OF SCIENCE IN NAVAL ARCHITECTURE
AND MARINE ENGINEERING
at the
MASSACHUSETTS INSTITUTE OF TECHNOLOGY
May 1963

H. H. WOODSON
THESIS SUPERVISOR

MHD FLOW IN A RECTANGULAR CHANNEL WITH APPLICATION TO A MARINE PROPULSION SYSTEM USING SUPERCONDUCTING MAGNETS

by

LIEUTENANT ROBERT A. DORAGH, U.S.N.
B.S., U.S. NAVAL ACADEMY
(1957)

SUBMITTED IN PARTIAL FULFILLMENT
OF THE REQUIREMENTS FOR THE
DEGREE OF NAVAL ENGINEER
AND THE DEGREE OF
MASTER OF SCIENCE IN NAVAL ARCHITECTURE
AND MARINE ENGINEERING
at the
MASSACHUSETTS INSTITUTE OF TECHNOLOGY

MHD FLOW IN A RECTANGULAR CHANNEL WITH APPLICATION TO A MARINE PROPULSION SYSTEM USING SUPERCONDUCTING MAGNETS BY ROBERT A. DORAGH, Lieutenant, U.S.N.

Submitted to the Department of Naval Architecture and Marine Engineering on 17 May 1963 in partial fulfillment of the requirements for the Master of Science degree in Naval Architecture and Marine Engineering and the Professional degree, Naval Engineer.

ABSTRACT

Marine propulsion using a screw propeller cannot couple large amounts of power quietly to sea water, and has the added disadvantage that the hull of the vehicle must always be pierced by a rotating shaft.

Marine propulsion using a magnetohydrodynamic pump-jet can be twenty decibels quieter than a screw propeller, compact, and free of underway maintenance problems. This type of propulsion device is feasible only with the use of superconducting magnets, but can be built with presently available technology.

The efficiency of conversion of electrical energy to motion of this device is calculated for a two thousand ton submarine at various speeds using the methods of the Naval Architect. It is assumed that magnetic flux densities up to twenty webers per square meter are available and that the conductivity of sea water is four mhos per meter. The results of these computations show that a MHD pump-jet's efficiency is limited by the hydraulic losses it experiences, but it has a relatively constant efficiency with speed for a specified geometry. An optimum geometry using a square channel would have a ratio of outlet to inlet velocity of 1.25, be approximately one hundred square feet in cross-section and fifty feet long. With a magnetic flux density of twenty webers per square meter such a device could have an efficiency of seventy percent which must be compared to an efficiency of eighty percent for a conventional propulsion system.

The refinements in present technology that would make such a propulsion device possible, and the areas for basic study are discussed. These are the effect on submarine drag of a pump-jet; the effect on turbulent fluid velocity profile of a magnetic field; the structure associated with superconductors in a dewar; the development of an efficient cryogenic system; and, finally, the development of a gas exhaust system to insure quiet operation of the device. The study concludes that there is no a priori reason why the possible characteristics of a MHD pump-jet cannot be achieved.

Thesis Supervisor: H. H. Woodson
Title: Associate Professor of Electrical Engineering

ACKNOWLEDGMENT

The author wishes to express his most sincere thanks to Professor H. H. Woodson who introduced him to the subject of magnetohydrodynamic energy conversion, suggested the study of an MHD pump used for marine propulsion, and gave encouragement, guidance, and advice throughout the preparation of this thesis.

The help extended by Commander J. R. Baylis, USN, in the many Naval Architectural problems; Professor P. S. Eagleson in the hydrodynamic analysis; and Mr. Z. J. Stekly of Avco-Everett Research Laboratory on superconductors and the structural problems of a dewar is greatly appreciated.

The interesting discussion with Professor H. P. Meissner on the electrolysis of sea water and the many other discussions with other members of the M.I.T. faculty are also appreciated.

The calculations in this work were done in part at the M.I.T. Computation Center, Cambridge, Massachusetts, on the IBM 7090 digital computer.

Finally, the author takes this opportunity to thank his wife, Patricia, for her patience, understanding, and heretofore unrecognized contributions to his academic work.

TABLE OF CONTENTS

LIST OF FIGURES

UNITS AND LIST OF SYMBOLS

Notes:

1. All Hydrodynamic equations are written using the English Units System.
2. All Electrical equations are written for the rationalized system of M.K.S. units.

Symbol	Definition
A	Channel Cross-Section Area
a	Characteristic Dimension
AR	Aspect Ratio
B	Magnetic Flux Density
B_o	Applied Magnetic Field
C_n	Arbitrary Constants (numbered)
c	Speed of Light
$D(\ )/Dt = \frac{\partial}{\partial t} + (\bar{u}.\bar{\nabla})$	Material Derivative
$D_H = \frac{4A}{P_E}$	Hydraulic Diameter
E	Electric Field
$f_n(\ )$	Arbitrary Function of ( ) (numbered)
$f'_n(\ )$	Derivative of $f_n(\ )$
f	Force Density
f_e	Electric Force Density
F	Force
g	Gravitational Acceleration
h	Specific Enthalpy
H_{L_n}	Hydraulic Loss at n
H_p	Pump Head Input
J	Current Density
k	Height of Boundary Roughness
K	Thermal Conductivity or Hydraulic Loss Coefficient

L	Characteristic Length
$M = B\,a\sqrt{\frac{\sigma}{\eta}}$	Hartmann Number
m	Mass
P_E	Perimeter of Channel Cross-Section
p	Local Pressure
q	Electric charge
Q	Flow Rate
$r = \frac{1}{\sigma}$	Electrical Resistivity
$R_E = \frac{U\,a}{\nu}$	Reynolds Number
$R^* = \frac{u^* a}{\nu}$	Shear Reynolds Number
$R_m = \mu_o \sigma a\, U$	Magnetic Reynolds Number
t	Time
T	Temperature or Thrust
u	Point, Time Mean Velocity
$u^* = \sqrt{\tau_o / \rho}$	Shear Velocity
U_o	Maximum Time Mean Velocity or Vehicle Speed
U_n	Bulk Mean Velocity at n
V	Applied Channel Voltage
w	Width of Channel
x, y, z	Orthoginal Directions
y	Distance From Boundary
$y^* = \frac{y\,u^*}{\nu}$	Local Reynolds Number
Z	Height Above Datum
Z_e	Electron Charge
$\alpha, \beta,$	Integration Variable to Account for Profile Variations
γ	Specific Weight
$\overline{\nabla} \times (\quad)$	Vector Cross-Product
$\overline{\nabla} \cdot (\quad)$	Vector Divergence
$\overline{\nabla}(\quad)$	Vector Gradient
ΔC_f	Added Drag For Shell Roughness
$\Delta(\quad) = (\quad)_2 - (\quad)_1$	

ϵ_o	Permitivity of Free Space
η	Viscosity
λ	Friction Factor
μ_o	Permeability of Free Space
ν	Kinematic Viscosity
ν_c	Collision Frequency
ξ	Non-Dimensional Distance from Wall
ρ	Mass Density
ρ_f	Electric Charge Density
σ	Electrical Conductivity
τ_o	Wall Shear Stress
$\phi = \rho g Z$	Gravitational Potential
Φ	Viscous Energy Density
χ	Non-Dimensional Distance from Centerline
$w_c = \frac{Z_e B}{c\ m}$	Cyclotron Frequency
$\epsilon_H, \epsilon_{EL}, \epsilon_{Total}$	Efficiencies
$\frac{\partial}{\partial(\ )}$	Partial Derivative
$\hat{i}_n$	Unit Vector in n Direction
$\underline{(\ )}$	Vector Quantity
$(\tilde{\ })$	Non-Dimensionalized Vector Quantity
$< >$	Bulk Time Average
$\rightarrow o$	Approaches Zero
$\not\rightarrow o$	Does not Approach Zero

I. INTRODUCTION

1.1 General

With the advent of shipboard nuclear reactors, deeper operating depths, and intricate weapons systems, submarines have become weight limited designs. This has occurred just at the time when significant advances are being made in tactics allowing the designer to concentrate on the hydrodynamic shape of the submarine and the higher underwater speeds this implies.

The military value of a submarine is found in four characteristics:

(a) Pay-load

(b) Maneuverability

(c) Speed

(d) Endurance

In a weight limited design, a compromise of these characteristics is necessary. The usual result of this is large size since this allows an adequate pay-load and endurance at the cost of speed and maneuverability. The ideal submarine would be so small that its cost in materials and manpower are minimal. Its propulsion system would not be limited by cavitation and would be so free from self-noise as to provide no impediment to the use of its weapons systems.

For over a decade, it has been clear that no presently used propulsion system can simultaneously be quiet, small, powerful, and be capable of the deeper depths increased maneuverability implies. It is basically for this reason that the pump-jet has been of interest to the Naval Architect.

It was not until the airplane was freed from its propeller that it was able to get a significant increase in speed without an enormous penalty in size; will this not also be so with the marine vehicle? Unfortunately such reasoning has always hit the blank wall of a marine pump that could not compete with the marine propeller in performance. It now appears that the magnetohydrodynamic

pump may be able to compete with the marine propeller, and, at the same time, offer many other advantages. Among these advantages are quiet operation provided by the lack of moving mechanical parts; increased power conversion to motion of vehicle since cavitation would not be initiated by a high speed rotating device; an energy converter that can (and probably must) be treated as a "black box", decreasing underway maintenance problems and personnel; and the fact that no rotating shaft need penetrate the pressure hull.

1.2 History of Problem

Ever since Faraday in 1831 and 1832 attempted to use the conductivity of the river Thames to measure tidal currents, the idea that is magnetohydrodynamics*) has been with us. Basically, MHD can be defined as the science of using a magnetic field to convert hydrodynamic energy to electrical energy and vice versa without any intervening mechanical device. Some prefer to think of MHD devices as machines in which the rotating element has been replaced by the flow of a fluid. This is a convenient way of approaching the MHD pump. In chapter II, the direct current MHD pump is described in analytical detail: it suffices here to say that in theory the MHD pump is a convenient and practical method of applying electrical power to a fluid for propulsive purposes. Yet, except for some relatively small devices, this type of energy conversion has not been used effectively.

Both Phillips **) (1) and Friauf (2) have detailed the reasons why the MHD pump has not been used as a marine propulsion system:

(a) Using permanent magnets, the efficiency of conversion of electrical power to motion is less than ten percent as compared to the eighty percent available with conventional methods.

---

*) For the obvious convenience, magnetohydrodynamics will be referred to as MHD.

**) Numbers in parentheses refer to bibliography.

(b) Using copper field coil magnets, this efficiency is not increased enough to make up for the ohmic losses in the coil.

(c) The weight of the coils is so excessive as to make the system prohibitive even if it were efficient.

(d) One basic reason for the poor efficiency is the low conductivity of sea water; to avoid this problem by seeding or some two fluid system is prohibitively expensive (if not impossible).

(e) The external magnetic fields caused by such a system would make the vehicle so detectable as to void any military value gained by the absence of mechanical devices and their inherent noise.

In addition to the problems of efficiency, weight, and detectibility, there is a considerable lack of information and understanding concerning the coupling of magnetic fields and turbulent fluid flows. Hartmann and Lazarus (3) were the first to investigate this coupling or interaction for flows in ducts of various geometries. Murgatroyd (4) in 1953 made pressure drop measurements for the flow of liquid mercury in a rectangular channel, and more recently Brouillette and Lykoudis (5) have examined the same problem, but at higher Reynolds numbers. As yet, there is no encompassing, illuminating theory of this interaction. This fact, and the limit of agreed-upon knowledge is discussed in Chapter III with special emphasis on rectangular channels with turbulent fluid flows. The important result for this particular problem, is that all discussions and computations must be restrained to rough estimates of what will actually occur in an MHD device because of the scarcity of experimental data.

This then is the "state of the art". Why examine the possibilities of MHD marine propulsion at this time? The reason is superconducting magnets.

1.3 Superconducting Magnets

Superconductivity was first noted by K. Onnes in 1911 in an experiment to measure the resistivity of mercury wire at low temperatures. As the name

superconductivity implies, this state of a metal is characterized by the loss of electrical resistivity. The resistivity of pure metals at low temperatures can be expressed approximately by:

$$r = r_T + r_i + r_B$$

where r_T is due to the thermal lattice vibrations, r_i is due to impurity effects and r_B is the magnetoresistance due to the presence of a magnetic field. None of the above functions vary linearily with temperature, impurity, or magnetic field, but can exhibit extremely marked changes. As the formulation implies, there is both a critical temperature and a critical magnetic field above which superconductivity cannot exist. This critical temperature and critical magnetic field is a property of the specific metal or alloy and cannot be accurately predicted by any present theory (6).

Even though a loss-free coil would have been of great interest many years ago, the fact that the critical fields of superconductors appeared to be less than a few kilogauss relegated the phenomenon to the position of a laboratory curiosity. Recently Kunzler (8) has shown that by cold working some superconductors, supercurrents can be maintained at fields as great as thirty times the "bulk critical magnetic field" *). Superconductors which have this property are referred to as "hard".**) In addition to this, it has been shown (9, 10) that β-tungsten structure compounds such as Nb_3Sn, V_3Si, and V_3Ga remain superconducting at fields up to ten webers per square meter, and there is evidence of critical magnetic fields in excess of fifty webers per square meter in the superconducting V-Ga system (11). These facts have led to a great deal of technical interest in loss-free superconducting magnets.

This type of magnet will increase the efficiency of a MHD pump without adding enormous weight for coils. It is also important to note that superconducting materials can be used to shield a magnetic field so that detectibility

---

*) This "bulk critical magnetic field" can be calculated using thermodynamic arguments (7).

**) Certain alloys and compounds are "hard" and will be referred to as alloy or compound superconductors.

is kept to a minimum.*) Therefore, of the previously stated disadvantages in the use of a MHD pump, only that concerning the conductivity of sea water remains. Chapter V will show that for high magnetic fields the conductivity of sea water is not a major consideration. Chapter VI will discuss the added structural problems that use of superconducting magnets will give; it can be stated now that there is reason to believe that this structure can be so optimized that its total weight will be within acceptable limits for use with a marine propulsion device.

1.4 Purpose and Subject of this Study

Considering what has been shown above, it is clear that there is sufficient reason to study the feasibility of using superconducting magnets with a MHD pump-jet as a propulsion system for a marine vehicle. Such a system will be the subject of this study. Figures I and II present a schematic view of the relative sizes of the device to be studied and the geometries involved. The expected characteristics of this device have been approximated as closely as possible; and the effects of various parameters on the electrical energy conversion efficiency of the device, as calculated with the aid of an IBM 7090 computer, have been studied. This work was done in part at the MIT Computation Center. A description of the methods used is contained in Chapter IV and the results are presented in Chapter V.

*) This is called the Meissner Effect and is described in (6) pp. 359.

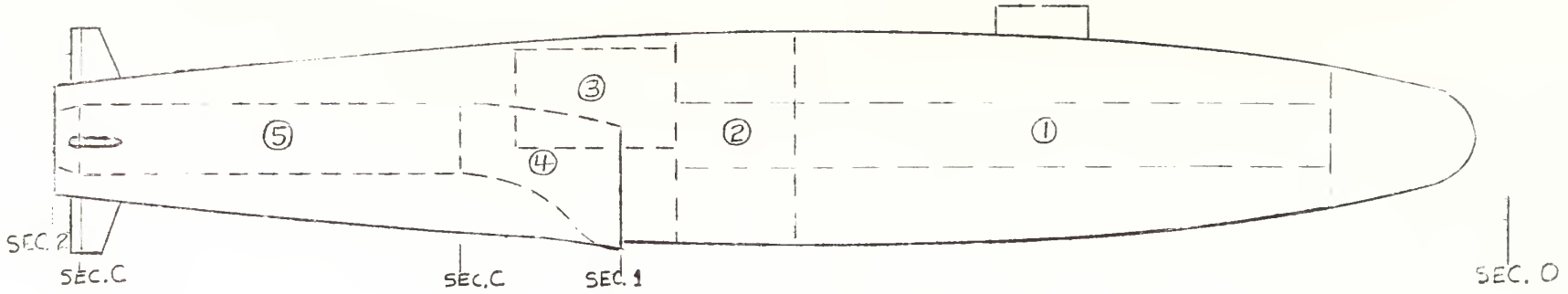

PROFILE VIEW

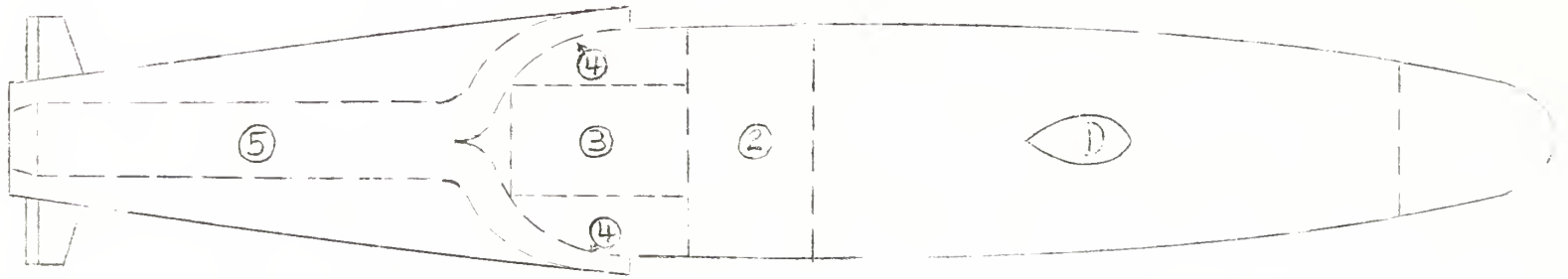

PLAN VIEW

FIGURE I
SCHEMATIC VIEW OF SUBMARINE WITH MHD PUMP-J .

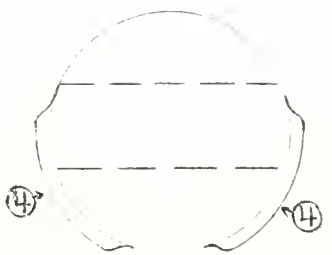

END VIEW

① LIVING AREA
② MACHINERY SPACE
③ REACTOR SPACE
④ INLET - DIFFUSER
⑤ MHD PUMP-JET

FIGURE II

SCHEMATIC VIEW OF MHD PUMP-JET

SUPPORTING STRUCTURE NOT SHOWN, STRUCTURE SIZE CAN BE ESTIMATED FROM PRESSURES AND TEMPERATURES.

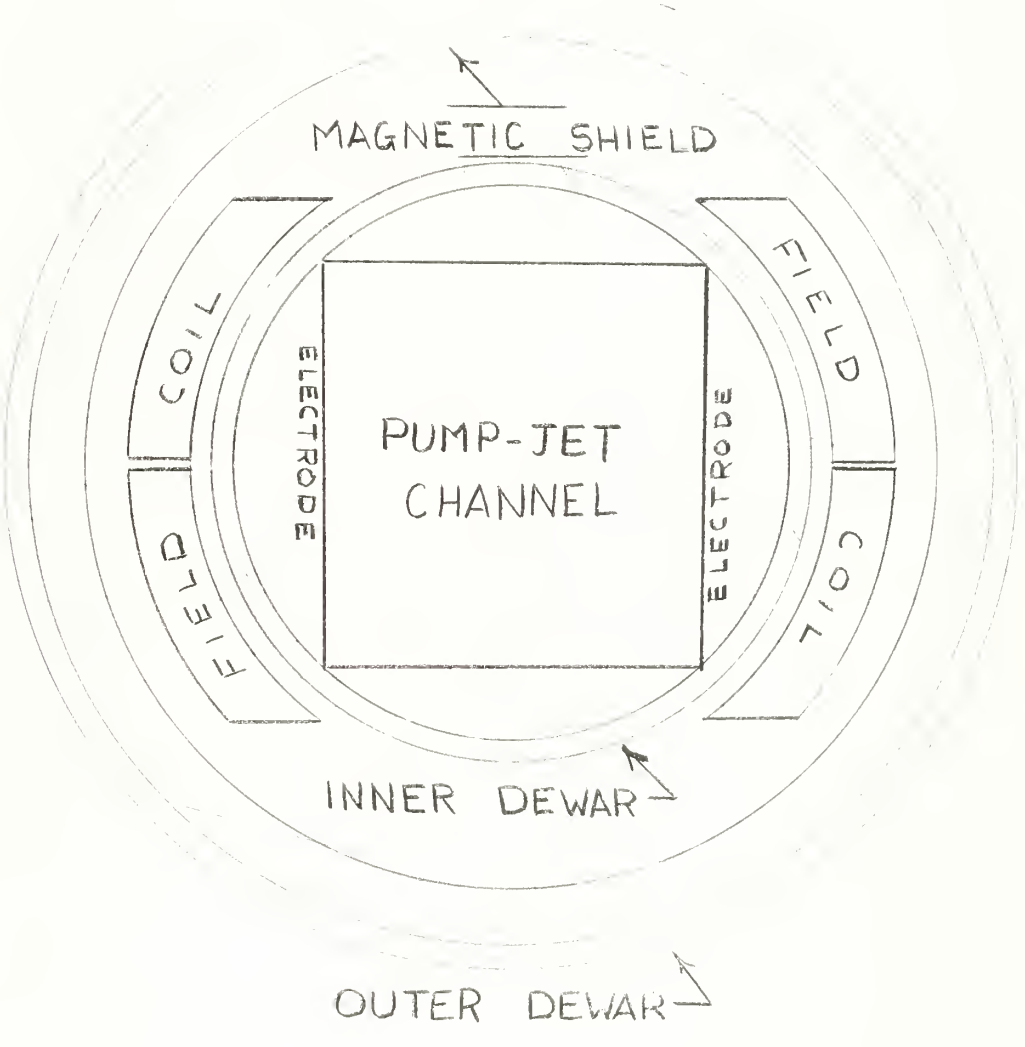

AMBIENT PRESSURE - 300°K

MAGNETIC PRESSURE - 4°K

VACUUM

II. Turbulent Hydromagnetic Flow In A Rectangular Channel

2.1 Importance of Subject

The rectangular channel is to the magnetohydrodynamist what the circular tube is to the ordinary hydrodynamist. It is a geometry in which a uniformity with dimension exists for the major parameters. In a circular tube, this uniformity is that of the symmetry of the velocity profile, which is for most applications the most important characteristic of hydrodynamic flow. In a rectangular channel, this uniformity is that of the applied magnetic and electric fields, the essence of MHD flow.

The importance of turbulent flows, of course, lies in the fact that almost all fluid flow problems with engineering interest are turbulent. But, despite this importance, turbulence has successfully defied analytic description and is approximated by engineers with semi-emperical methods which have dimensional analysis and analysis of laminar flow as their bases.

Although Harris (12) has applied these semi-emperical methods to turbulent MHD flows, some of his results do not agree with the methods of ordinary hydrodynamics or recent results of Brouillette and Lykoudis (5). Therefore, the semi-emperical method will be reviewed here to develop equations which emphasize rectangular channel flows and agree with ordinary hydrodynamics and recent results.

2.2 The Dimensional Analysis of Millikan (13)

For ordinary hydrodynamic flow in a closed duct there are two basic assumptions:

(a) Prandtl's Wall Velocity Law:

$$\lim_{y \to o} \frac{u}{u^*} = f_1 \left(y^*, {}^{y}/k\right)$$

if the wall is smooth:

$$\lim_{y \to o} \frac{u}{u^*} = f_2 (y^*) \qquad [1]$$

if the wall is rough:

$$\lim_{y \to o} \frac{u}{u^*} = f_3 (y/k)$$

Note that this formulation is independent of cross-section shape or distance from the centerline of the flow. It is applicable only for turbulent flow and therefore does not hold in the laminar sub-layer.

(b) Von-Karman's Velocity Defect Law:

$$\lim_{\eta \to o} \frac{U_o - u}{u^*} = f_4 (\eta) \qquad [2]$$

Note that this expression applies throughout the flow except near the walls, and may depend on the cross-section shape.

It is convenient at this time to state what is smooth and what is rough. Schlichting (14) shows that the flow very near the boundary is laminar if $y^* < 5$. Since it is the purpose of this analysis to examine turbulent flow, that section of a flow which is laminar is of interest only in as far as it describes the boundaries of the turbulent region. Therefore, if the roughness is such that it is completely within the laminar region, it will not effect the turbulence and is of no interest i.e. $k \leq \frac{5\,\vartheta}{u^*}$. Normally steel ducts (k = .00015 in.), with diameters of only a few inches have a laminar sub-layer thick enough to always contain the roughness. Therefore only smooth flows will be considered.

The boundary conditions on a fluid flow in addition to smoothness or roughness are:

(a) Velocity is zero at any wall.

(b) The derivative of the velocity with distance normal to the main flow is zero on the axis of symmetry.

(c) The velocity on the centerline is fixed by external conditions, such as the maximum free-stream velocity.

For the majority of applications, the engineer is interested in only two characteristics of a fluid flow; pressure drop and bulk rate of flow. By a force balance, the pressure drop along a flow is defined as:

$$(\Delta p) = \frac{\tau_o P_e L}{A}$$

The wall shear is non-dimensionalized by a characteristic velocity to define a friction factor:

$$\lambda = \frac{8 \tau_o}{\rho U_o^2}$$

It can be shown that (13):

$$\lambda = f_5(R_E, k/a)$$

or for smooth flow

$$\lambda = f_6(R_E)$$

Using these assumptions and definitions, Millikan has arrived at the following equations for ordinary hydrodynamic flow in a closed duct:

$$\frac{u}{u^*} = C_1 \left[\ln R^* \xi + C_2 + f_7(\xi) \right]$$

$$\frac{U_o - u}{u^*} = C_1 \left[\ln \frac{1}{\xi} - f_7(\xi) + f_7(1) \right]$$

$$\frac{1}{\sqrt{\lambda}} = \frac{C_1}{\sqrt{8}} \left[\ln (R_E \sqrt{\lambda}) + C_2 + f_7(1) - \frac{1}{2} \ln 8 \right]$$

where $f_7(1)$ can be a function of boundary shape as well as ξ and C_1 and C_2 are constants to be determined.

It is interesting to note that, as will be shown, this form of the solutions is universally used, but it is inconsistent with the boundary conditions as previously specified since:

$$\frac{du}{d\xi} = 0 \text{ when } \xi = 1$$

$$\frac{du}{d\xi} = u^* C_1 \left[\frac{1}{R^* \xi} + f'_7(\xi) \right]$$

$$f'_7(\xi) = \frac{d(f_7(\xi))}{d(\xi)} = -\frac{1}{R^* \xi}$$

$$f_7(\xi) = - \ln \xi + f_7(1)$$

Note that $f_7(\xi) \not\to o$ as $\xi \to o$ as required equation [1]* and its independence of shape. When this form of $f_7(\xi)$ is applied to [2]

$$\frac{U_o - u}{u^*} \not\to o \text{ as } \xi \to 1$$ as would be required by the symmetry of the problem. It is for these reasons that the boundary condition requiring zero slope of the velocity profile on the axis of symmetry is ommitted when the constants are defined.

2.3 The Electrical Effects Analysis of Harris (12)

The basic equations of steady, uncompressible MHD flow are:**

$$\bar{\nabla} \times \bar{E} = - \frac{\partial \bar{B}}{\partial t}$$

$$\bar{\nabla} \times \bar{B} = \mu_o \bar{J}$$

$$\bar{\nabla} \cdot \bar{B} = o$$

$$\bar{J} = \sigma (\bar{E} + \bar{u} \times \bar{B})$$

$$\bar{\nabla} \cdot \bar{u} = o$$

$$\rho \frac{D\bar{u}}{Dt} = -\bar{\nabla} p + \eta \nabla^2 \bar{u} + \bar{J} \times \bar{B}$$

If a characteristic velocity, length, and magnetic field are determined these equations can be non-dimensionalized such that:

$$\tilde{\nabla} \times \tilde{E} = - \frac{\partial \tilde{B}}{\partial \tilde{t}}$$

$$\tilde{\nabla} \times \tilde{B} = R_m \tilde{J}$$

$$\tilde{\nabla} \cdot \tilde{B} = o$$

---

*) Numbers in brackets refer to equations.

**) For derivation see Chapter III and any basic field theory text.

$$\tilde{J} = \tilde{E} + \tilde{u} \times \tilde{B}$$

$$\tilde{\nabla} \cdot \tilde{u} = 0$$

$$\frac{D\tilde{u}}{D\tilde{t}} = -\tilde{\nabla}\tilde{p} + \frac{1}{R_E}\tilde{\nabla}^2 \tilde{u} + \frac{M^2}{R_E}(\tilde{J} \times \tilde{B})$$

It is important to note that only two new non-dimensional parameters appear in these equations:*

1. Magnetic Reynolds number, which appears in Ampere's Law and is a measure of the diffusion rate of the magnetic field.
2. Hartmann number which is a measure of the effect of forces of electrical origin on the kinetic energy of a flow.

Harris shows that $\frac{u}{u^*} = f_8(y^*, M, \tilde{\xi})$ for flow in a smooth closed duct and that this functional relationship can be reduced to:

$$\left[\frac{u}{u^*}\bigg|_{M\neq o} - \frac{u}{u^*}\bigg|_{M=o}\right] = f_9\left(\frac{M^2\tilde{\xi}}{R^*}\right) + f_{10}\left(\frac{M}{R^*}\right)$$

$$\left[\frac{1}{\sqrt{\lambda}}_{M\neq o} - \frac{1}{\sqrt{\lambda}}_{M=o}\right] = \frac{1}{\sqrt{8}} f_{10}\left(\frac{M}{R^*}\right) + \frac{R^*}{\sqrt{8M^2}} \int_o^{M^2/R^*} f_9\left(\frac{M^2\tilde{\xi}}{R^*}\right) d\left(\frac{M^2\tilde{\xi}}{R^*}\right)$$

In summary, dimensional analysis produces the following form of the equations of hydromagnetic flow:

$$\frac{u}{u^*} = C_1\left[\ln R^*\tilde{\xi} + C_2 + f_7(\tilde{\xi})\right] + f_9\left(\frac{M^2\tilde{\xi}}{R^*}\right) + f_{10}\left(\frac{M}{R^*}\right)$$

$$\frac{U_o - u}{u^*} = C_1\left[\ln\frac{1}{\tilde{\xi}} - f_7(\tilde{\xi}) + f_7(1)\right] - f_9\left(\frac{M^2\tilde{\xi}}{R^*}\right) + f_9\left(\frac{M^2}{R^*}\right)$$

$$\frac{1}{\sqrt{\lambda}} = \frac{C_1}{\sqrt{8}}\left[\ln(R_E\sqrt{\lambda}) + C_2 + f_7(1) - \frac{1}{2}\ln 8\right] + \frac{1}{\sqrt{8}} f_{10}\left(\frac{M}{R^*}\right)$$

$$+ \frac{R^*}{\sqrt{8}\,M^2} \int_o^{M^2/R^*} f_9\left(\frac{M^2\tilde{\xi}}{R^*}\right) d\left(\frac{M^2\tilde{\xi}}{R^*}\right)$$

It is now necessary to examine laminar flow analysis and test data in order to attach importance to the above factors and to evaluate the constants.

---

*) R_E, Reynolds number appears alone in this form of the Navier-Stokes equation if $\tilde{J} \times \tilde{B} = o$.

2.4 Analysis of Laminar Flow In A Rectangular Closed Channel

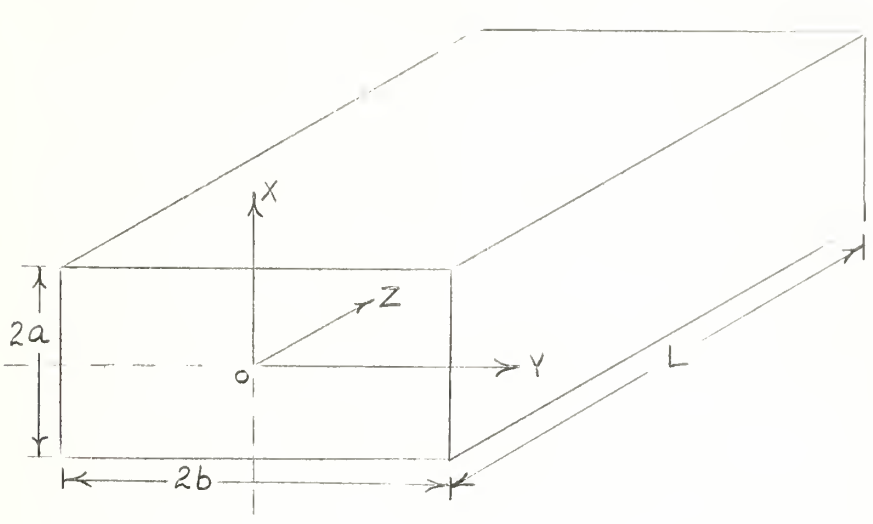

In the absence of forces of electrical origin, steady, incompressible flow in a rectangular channel has as its basic equation of motion:

$$\rho\,(\bar{u}.\bar{\nabla})\,\bar{u} + \bar{\nabla}p = \eta\,\nabla^2\bar{u}$$

if velocity is constrained to be one-dimensional in the z direction:

$$\nabla^2_{x,y}\,\bar{u}_z + k = o$$

where k is a constant derived from a force balance such as:

$$(\Delta p)A = -P_E\,\eta\,\frac{du}{d\xi}\,L$$

$$\nabla p = \frac{\Delta p}{L} = -\left(\frac{P_E}{A}\,\frac{du}{d\xi}\right)\eta = -k\,\eta$$

The homogeneous solution of the equation of motion is:

$$(u_z)_H = (A\,e^{-\alpha x} + B\,e^{-\alpha x})\,(C\cos\alpha y + D\sin\alpha y)$$

The particular solution can be found by the convenient substitution:

$$k = k\,\frac{4}{\pi}\sum_{o}^{\infty}\frac{(-1)^n}{(2n+1)}\cos\frac{(2n+1)\,\pi y}{2\,b}$$

which when applied to the equation of motion has the solution:

$$(u_z)_p = \frac{16\, k\, b^2}{\pi^3} \sum_{o}^{\infty} \frac{(-1)^n}{(2n+1)^3} \cos \frac{(2n+1)\,\pi y}{2b}$$

Therefore, the general solution is:

$$u_z = (A\, e^{\alpha x} + B\, e^{-\alpha x})(C \cos \alpha y + D \sin \alpha y) + \frac{16\, k\, b^2}{\pi^3} \sum_{o}^{\infty} \frac{(-1)^n}{(2n+1)^3} \cos \frac{(2n+1)\,\pi y}{2\, b}$$

Applying the boundary conditions:

(a) $u_z = o$ on all walls

(b) $\frac{\partial u_z}{\partial x} = o$, $x = o$

(c) $\frac{\partial u_z}{\partial y} = o$, $y = o$

The solution reduces to:

$$u_z = \frac{16\, k\, b^2}{\pi^3} \sum_{o}^{\infty} \frac{(-1)^n}{(2n+1)^3} \left[1 - \frac{2 \cosh \alpha\, x \sinh \alpha a}{\sinh (2\alpha a)} \right] \cos \frac{(2n+1)}{2b} \pi y \qquad [3]$$

where $\alpha = \frac{(2n+1)\pi}{2b}$

Shercliff (15) has analyzed steady incompressible flow in a rectangular channel in the presence of forces of electrical origin, and has arrived at the following solution:

$$u_z = \frac{16\, k\, b^2}{\pi^3} \sum_{o}^{\infty} \frac{(-1)^n}{(2n+1)^3} \left[1 + \frac{\cosh s_1 x \sinh s_2 a - \cosh s_2 x \sinh s_1 a}{\sinh (s_1 - s_2)\, a} \right] \cos \frac{(2n+1)\pi y}{2\, b} \qquad [4]$$

where s_1 and s_2 are roots of

$$s^2 + Ms/a - \frac{(2n+1)^2\, \pi^2}{4\, b^2} = o$$

The Laminar solutions for flow in a circular tube are:

(a) Without electrical effects (M = 0):

$$u_z = \frac{k}{4} (a^2 - y^2)^{1/2} \qquad [5]$$

(b) With electrical effects (M = 0):

$$u_z = \frac{k}{4} \frac{a}{M} (a^2 - y^2)^{1/2} \qquad [6]$$

From a comparison of [3, 4, 5, 6] it is significant that:

(a) The laminar solutions are dependent on the shape of the cross-section.

(b) Of the two functions introduced by Harris, only $f_{10}(\frac{M}{R^*})$ occurs.

(c) In the rectangular section solution, the effect of the electrical forces varies across the section, but in the circular section, it appears as a multiplicative constant.

2.5 Observations of Turbulent Hydrodynamic and Hydromagnetic Flows and Their Semi-Emperical Equations

At the present time, there are three sources of data on hydromagnetic flow (3, 4, 5). All of these sources have measured only the bulk average velocity and length pressure drop of the flow. Although Brouillette and Lykoudis (5) have stated that their next report will contain velocity profile measurements, there now exists no published data on velocity profiles in MHD flow. Nevertheless, Harris (12) has suggested a complete set of equations to describe turbulent MHD flow which are as follows:

$$\frac{1}{\sqrt{\lambda}} = 2.0 \log_{10}(R_E \sqrt{\lambda}) - 0.8 + \frac{1}{\sqrt{8}} \int_0^1 f_9 \left(\frac{4\sqrt{8}\, M^2 \chi}{R_E \sqrt{\lambda}} \right) d\chi$$

$$\frac{u}{u^*} = 5.657 \log_{10}(R^* \chi) + 6.154 + f_9(M^2/R^*)$$

$$\frac{1}{\sqrt{8}} \int_0^1 f_9 \left(\frac{4\sqrt{8}\, M^2 \chi}{R_E \sqrt{\lambda}} \right) d\chi = 0.547 - 2.0 \log_{10}\left(\sqrt{8} \left(\frac{u^*}{U} \right)^2 \right) + \frac{R^*}{\sqrt{8}\, M^2} \int_0^{M^2/R^*} f_9 \left(\frac{M^2 \chi}{R^*} \right) d\left(\frac{M^2 \chi}{R^*} \right)$$

$$\frac{R^*}{\sqrt{8}\, M^2} \int_0^{M^2/R^*} f_9 \left(\frac{M^2 \chi}{R^*} \right) d\left(\frac{M^2 \chi}{R^*} \right) = 0.135 - 2 \log_{10}\left(\frac{M^2}{R^*} \right) - \frac{R^*}{\sqrt{8}\, M^2} \quad \text{if } \frac{M^2}{R^*} \geq 0.6$$

$$= .1 \sin\left(\frac{M^2/R^* \pi}{.57} \right) \quad \text{if } \frac{M^2}{R^*} < 0.6$$

$$f_9\left(\frac{M^2}{R^*}\right) = -2.07 - 5.657 \log_{10}\left(\frac{M^2}{R^*}\right) \quad \text{if} \quad \frac{M^2}{R^*} \geq 0.6$$

$$= 1.557\, M^2/R^* \cos\left(\frac{M^2/R^*\,\pi}{.57}\right) + .28 \sin\left(\frac{M^2/R^*\,\pi}{.57}\right) \quad \text{if} \quad \frac{M^2}{R^*} < 0.6$$

$$R^* = \sqrt{\frac{\lambda}{8}}\ \frac{R_E}{4}$$

It is important to note that:

(a) $f_{10}\left(\frac{M}{R^*}\right)$ does not appear in these equations as indicated by the laminar solutions.

(b) Regardless of the cross-section or Reynolds number there is no variation in the effect of the electrical forces across the section as is indicated in the laminar solution in a rectangular channel.

(c) There is no $f_7(\xi)$ function as suggested by Millikan's analysis.

(d) χ measures distance from the centerline as opposed to distance from the wall. The normal method is to measure distance from the nearest wall since this is what has been assumed when [1] is used.

(e) The method of calculating R* is not that which is usually used since:

$$R^* = \frac{a\ u^*}{\nu} = \frac{1}{2}\ \frac{D_H\ U}{\nu}\ \frac{u^*}{U} = \frac{D_H\ U}{2\,\nu}\sqrt{\frac{\lambda}{8}} = \frac{R_E}{2}\sqrt{\frac{\lambda}{8}}$$

and:

$$\lambda = \frac{8\ \tau_0}{\rho\ U^2} = 8\left(\frac{u^*}{U}\right)^2$$

There are numerous sets of data at various Reynolds numbers for hydrodynamic flow in a circular tube, but those of Nikuradse (16) are perhaps the most widely known and will therefore be used in the following comparisons. The data for hydrodynamic flow in a rectangular duct is much more limited, but that which exists is complete in both velocity profile and pressure drop measurements. For purposes of this analysis, the data of Hoagland (17) and Laufer (18) will be used.

Nikuradse has suggested complete equations to describe hydrodynamic flow. These equations are as follows:

$$\frac{1}{\sqrt{\lambda}} = 2.0 \log_{10} R_E \sqrt{\lambda} - 0.8$$

$$\frac{u}{u^*} = 5.75 \log_{10} R^* \xi + 5.5$$

Laufer has suggested a different set of constants for those given above:

$$\frac{u}{u^*} = 6.9 \log_{10} R^* \xi + 5.5$$

It is important to note that:

(a) There is no $f_7(\xi)$ function as suggested by Millikan's analysis.

(b) ξ measures a distance from the nearest wall as required by Prandtl's wall velocity law.

Although, as noted above, there is no $f_7(\xi)$ function in any of the above equations by Harris or Nikuradse, there is a shape parameter implicit in R^*, χ, and ξ since the characteristic length used in these parameters is a hydraulic radius which does depend on the shape of the cross-section:

$$R_H = \frac{2A}{P_E} \qquad D_H = 2 R_H \qquad R_E = \frac{D_H U}{\nu}$$

$$\xi = \frac{y}{R_H} \qquad \chi = \frac{R_H - y}{R_H}$$

It is for this reason, as will be shown, that these methods of representation of pressure drop and velocity profile can be successful, regardless of the cross-section shape.

2.6 Comparison of Existing Equations as They Apply to Turbulent Hydrodynamic Flow

It has been shown that the equations for turbulent MHD flow are the same as those for hydrodynamic flow with some additional terms. It is therefore, important to settle on a set of equations that adequately describe hydrodynamic flow. In order to do this, the equations as suggested by Harris (12) with M = 0

FIGURE III

Plot of Velocity Profile for Circular Tube

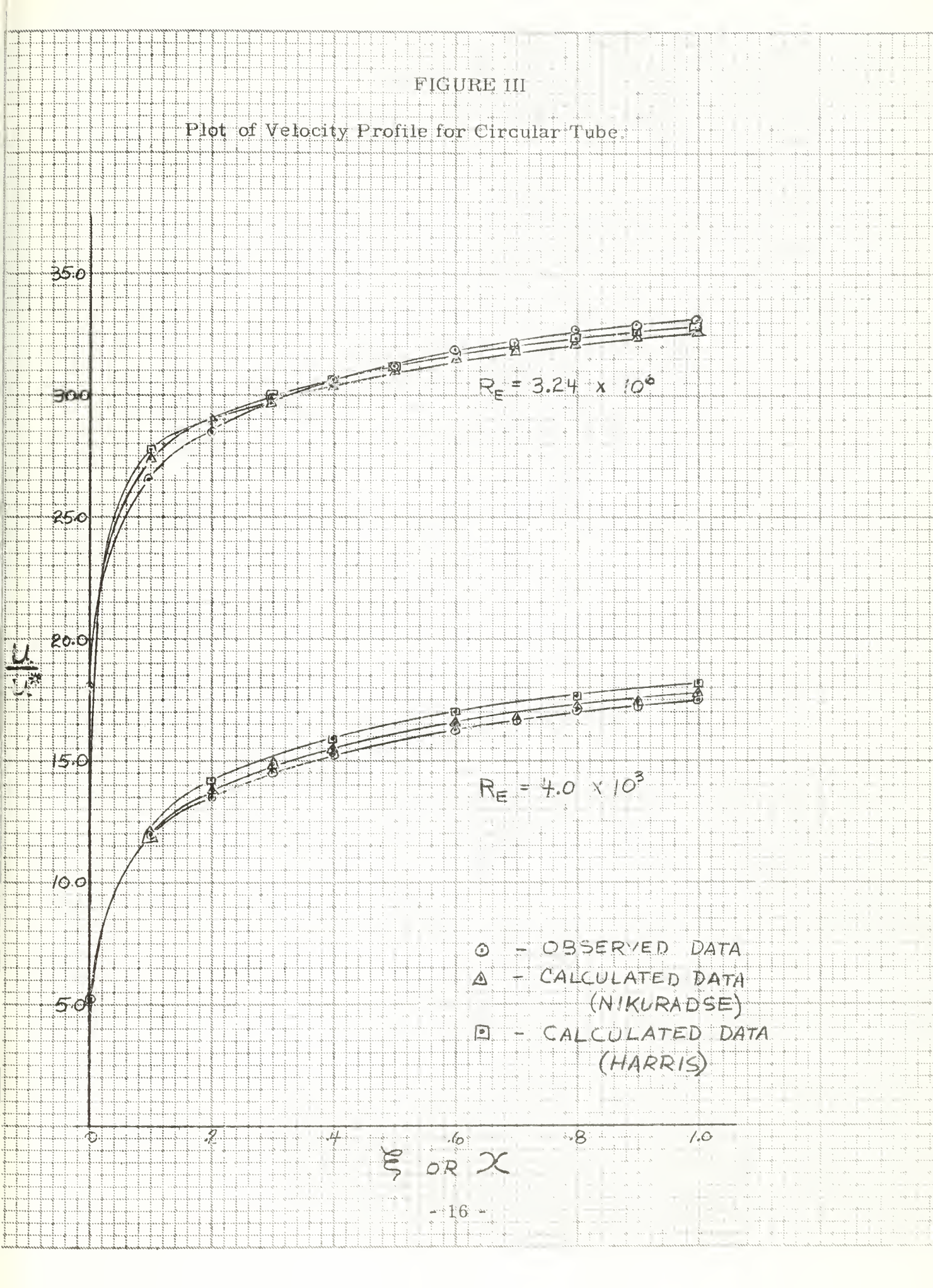

FIGURE IV

Plot of Velocity Profile for Square Channel

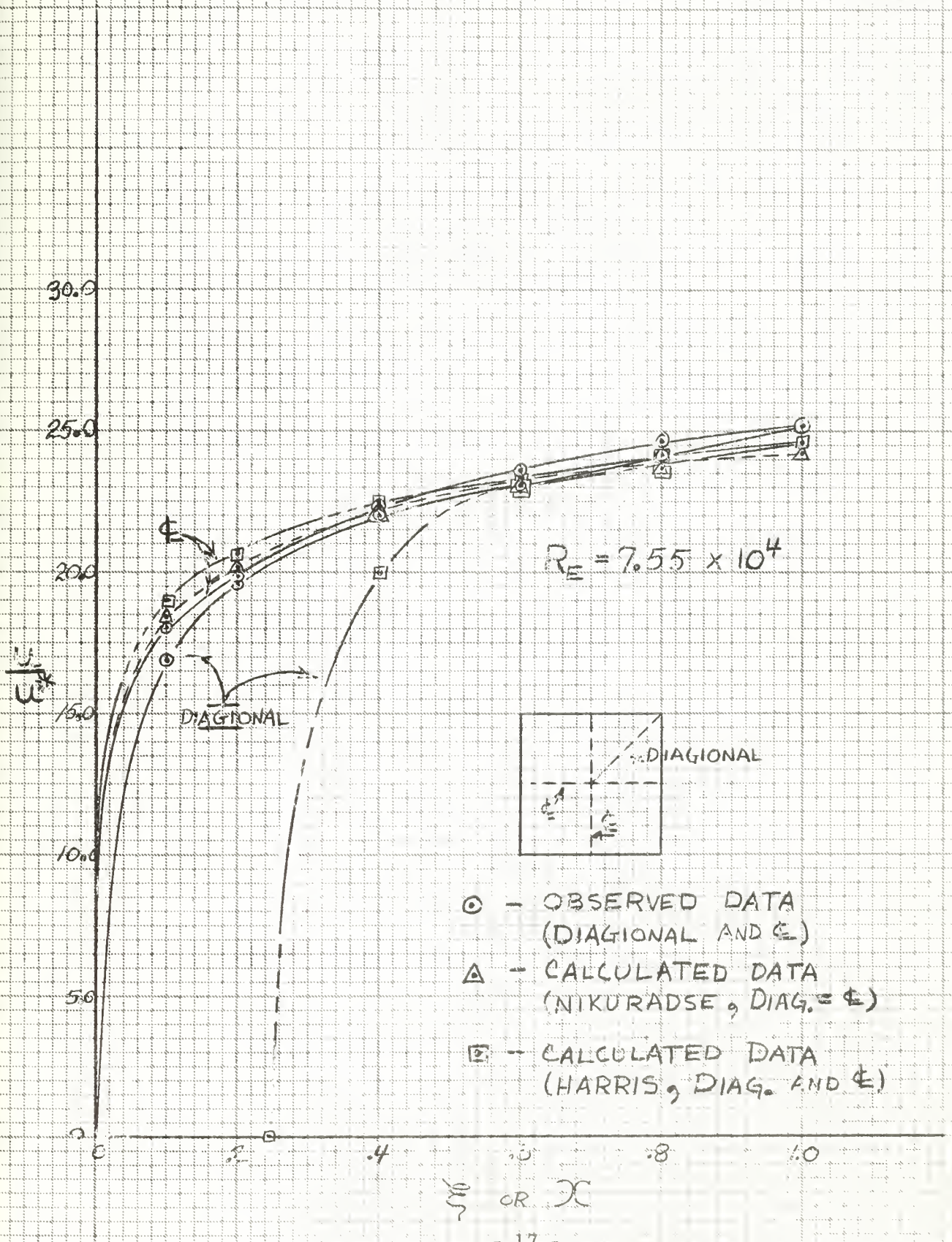

Figure V

Plot of Velocity Profile for Rectangular Channel, Aspect Ratio Two.

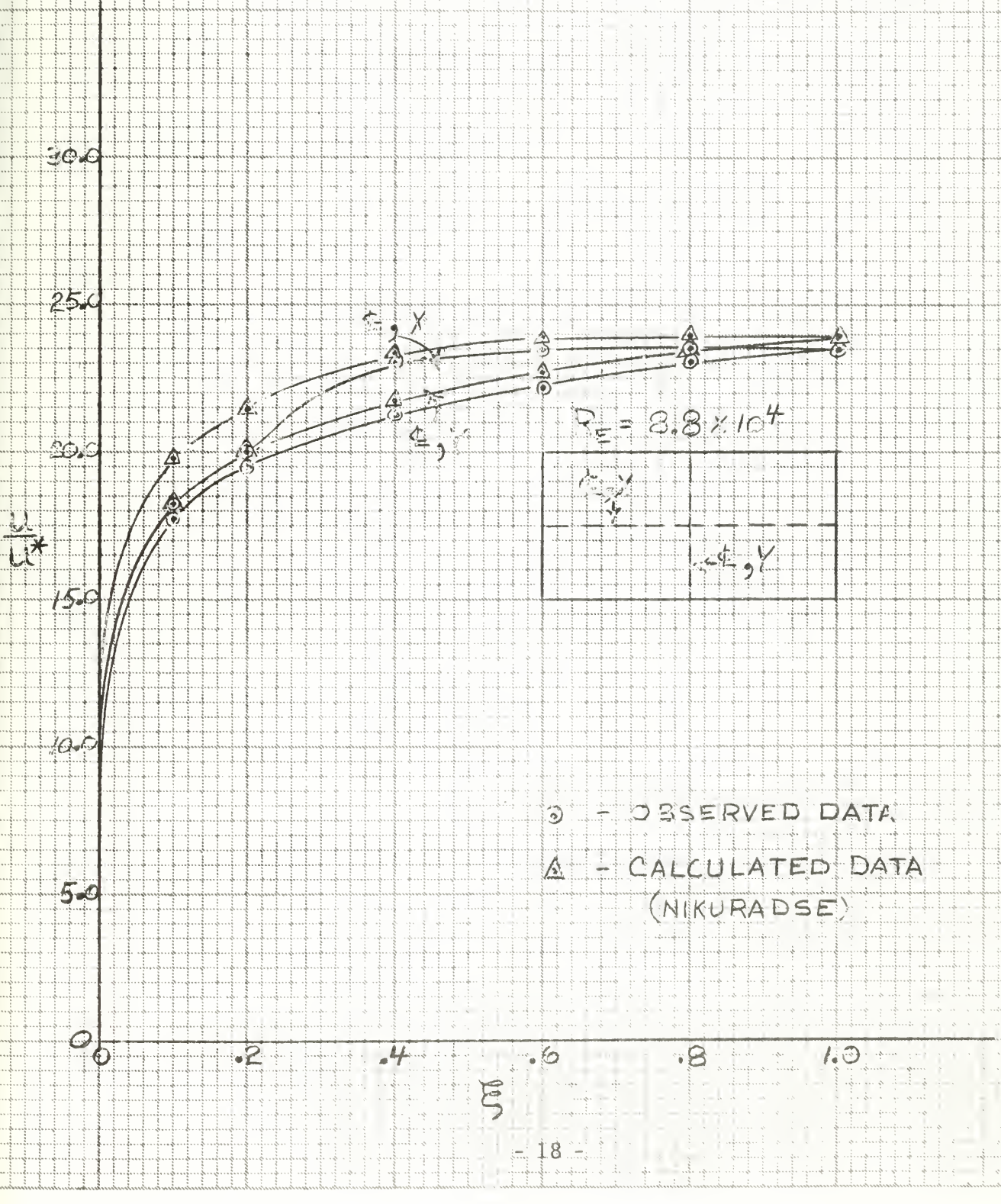

FIGURE VI

Plot of Velocity Profile for Rectangular Channel, Aspect Ratio Twelve

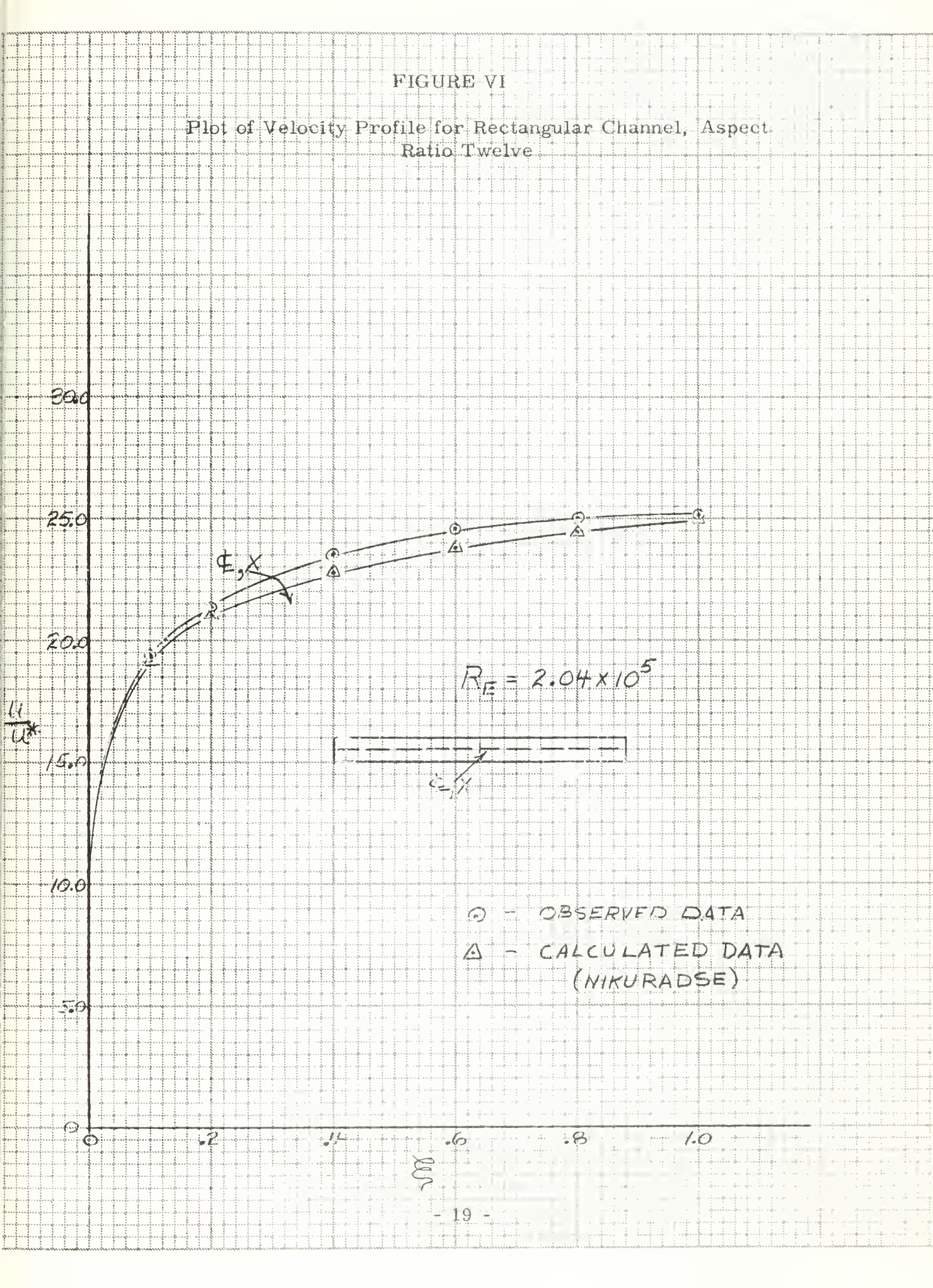

will be compared with those suggested by Nikuradse for:

(1) Flow in a circular tube (Fig. III)

(2) Flow in a square duct (Fig. IV)

(3) Flow in a duct of Aspect Ratio Two (Fig. V)

(4) Flow in a duct of Aspect Ratio Twelve (Fig. VI)

The observed data used as a standard is for:

(1) Circular tube -- Nikuradse (16)

(2) Ducts of Aspect Ratio One and Two -- Hoagland (17)

(3) Duct of Aspect Ratio Twelve -- Laufer (18)

These results will then be compared with those available by using Laufer's equations and those which would be obtained by using a set of equations which are of the form suggested by Millikan.

2.7 Results of Comparison of Velocity Profiles

Figure III shows that either representation (Harris' with distance from the centerline or Nikuradse with distance from the nearest wall) adequately represents the velocity profile in a circular duct. These calculated results using Harris' equation have

$$R^* = \frac{R_E}{2}\sqrt{\frac{\lambda}{8}}$$

and not

$$R^* = \frac{R_E}{4}\sqrt{\frac{\lambda}{8}}$$

as suggested by Harris. If the latter method were used the results would be reduced uniformly by $5.657 \log_{10} 2.0$ which is 3.5 units on the scale used and would represent a 10% error for Reynolds numbers of the order of 10^6.

Figure IV shows that Nikuradse's equation agrees quite well with the velocity profiles as observed on the centerline and diagonals of a square channel. Harris' equation agrees well with the centerline velocity profile, but it is in poor agreement with the diagonal velocity profile. The reason for this last re-

FIGURE VII

Plot of Observed Isovels in Rectangular Channel

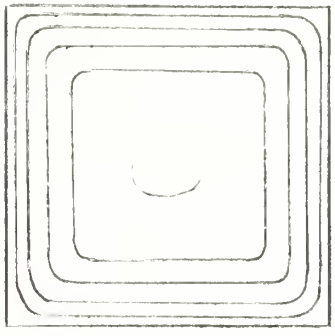

ASPECT RATIO ONE

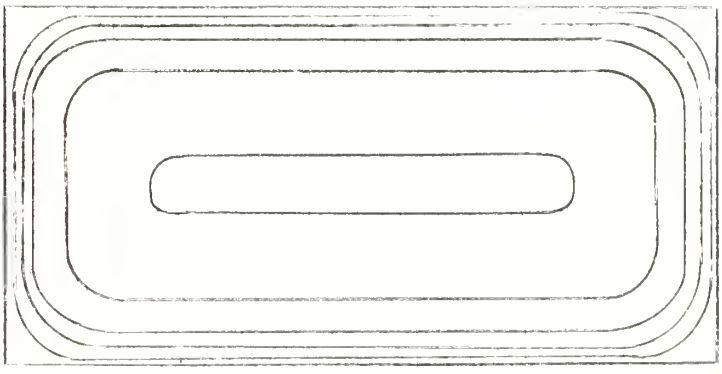

ASPECT RATIO TWO

FIGURE VIII

Plot of Calculated Isovels in Rectangular Channel

ASPECT RATIO ONE

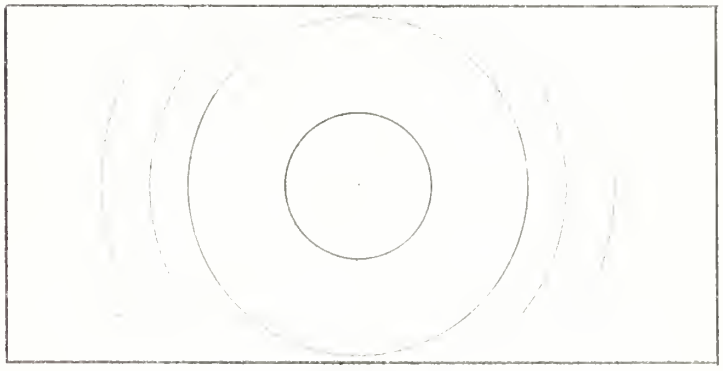

ASPECT RATIO TWO

sult is the method of measuring distances from the centerline of the duct.

Figure VII shows a typical isovel plot of the observed flow in a square channel. Figure VIII shows an isovel plot of the calculated flow in a square channel measuring distances from the centerline. It is clear that the symmetry this causes is not representative of the actual flow symmetry and cannot be permutted to accomplish any more than a decrease in the mean square error. It is for this reason that the method of Harris will not be used in the remaining discussion.

Figures V and VI show that Nikuradse's equation for velocity profiles agrees well with observed data. The bulge in the observed velocity profile is caused by secondary flows in the edges of the flow and is not represented by the present method of calculating the velocity profile. It is interesting to note that Nikuradse's equation is close enough to the velocity profile observed by Laufer to make one wonder why, on a sample point of three, it was necessary to change the constants involved in the profile calculations. Because of this, Nikuradse's equation will be used along with his constants to the exclusion of all others.

Is it possible to calculate a more accurate profile that follows the form of Millikan's analysis? An attempt to do this, has produced the following solution at the expense of much effort:

$$\frac{u}{u^*} = 2.44 \left[\ln R^* \xi + (1.4 + 8e^{-AR}) \left(1 + \sin \frac{(2\xi - 1.)\pi}{2}\right) - .62 \right]$$

where: $\xi = \dfrac{\sqrt{x^2 + y^2}}{1.75\, y_o}$

x, y = distance from wall

y_o = semi-width of narrowest dimension

It is doubtful if use of this equation is justified because:

(a) It is based on only the ten flows examined by Hoagland

(b) Nikuradse's equation is very close in accuracy to the degree of uncertainty in the velocity profile measurements and therefore any higher accuracy is suspect.

In summary:

FIGURE IX

Plot of Observed Friction Factors as a Function of M/R_E

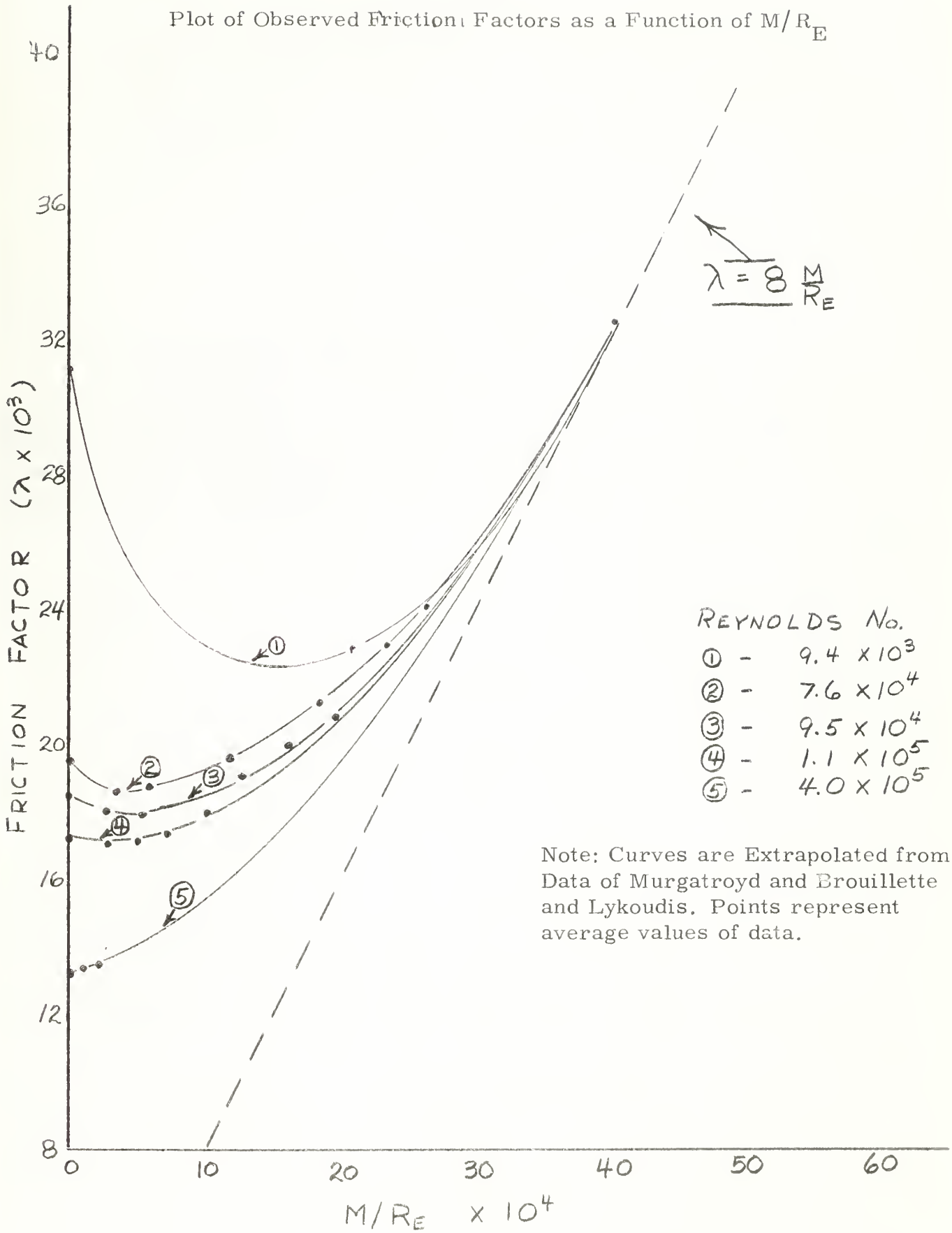

(a) Nikuradse's velocity profile equation adequately represents observed hydrodynamic flow in both circular and rectangular ducts.

(b) There are no data now available on velocity profile in turbulent MHD flow; therefore no attempt will be made to extend the previously discussed semi-emperical method to the evaluation of constants and the form of f_9 and f_{10}.

(c) Harris' equation for MHD flow are suspect in their hydrodynamic origins and their relationship to the laminar flow solutions.

2.8 Results of Comparison of Friction Factors

There is no disagreement among authorities that Nikuradse's equation for friction factor adequately represents observed data for hydrodynamic flow. Therefore this will not be discussed further. What is to be discussed is the form of this equation for MHD flow.

Figure IX is a plot of some of the observed data of Murgatroyd *) and Brouillette and Lykoudis for observed friction factors as a function of M/R_E. Brouillette and Lykoudis point out that their data are specifically in disagreement with the predictions of Harris in that at high Reynolds numbers there is no decrease in friction factor because of the application of the magnetic field (5).

From the data now available, curves of constant Reynolds number have been drawn and these curves extrapolated for the cases where little data exist. A few of these curves are shown on Figure IX. These curves tend to show that:

(a) The friction factor for MHD flow is primarily dependent on M/R_E since regardless of the Reynolds number, at high M/R_E, $\lambda = 8\ M/R_E$.

---

*) Murgatroyd has published his data (4) with the following definitions:

$$R_E = \frac{4\,d\,U\,\rho}{\eta} \qquad M = d\,B\sqrt{\frac{\tau}{\eta}}$$

where d (the characteristic dimension) is the semi-width of the narrowest dimension. This is an approximation of D_H which is 3.74 d for this case (aspect ratio 15:1). It is important that the 4 does not appear in the definition of M and therefore, if a consistent characteristic dimension is to be used, M must be multiplied by four. Harris has used R_E and M as Murgatroyd defined them. It is this inconsistency which accounts for Harris' inability to make Hartmann's and Lazarus' zero field data agree with Murgatroyd's for Nikuradse's equation (12).

(b) At low Reynolds numbers up to $R_E = 10^5$, there is a definite decrease in λ for M/R_E of the order of 10^{-3}.

In all fluid flows, a momentum transfer must exist from the center of the flow to the boundary since the momentum at the boundary in the flow must be zero, but that at the center is finite. For the low momentum flows called laminar, the viscous shear type of momentum transfer is enough to accomplish the momentum transfer. When a magnetic field is applied to this flow, eddy currents are generated in the flow adding an $I^2 R$ loss mechanism and therefore causing the larger friction factors, described by Hartmann and Lazarus (3). For the high momentum flows called turbulent, the viscous shear mechanism is too slow and an extremely "lossy" eddy diffusion occurs which transfers mass and momentum between the center and boundary of the flow. It is the randomness of this transfer which characterizes turbulence. When a magnetic field is applied to this flow, the $\bar{J} \times \bar{B}$ forces act to prevent this mass transfer at the same time adding the $I^2 R$ loss mechanism. There are experimentally observed conditions where this results in a decrease in losses, but, in general, the additional loss mechanism exceeds the gains of the lessening of the mass transfer resulting in the form of the curves shown in Figure IX.

Using these data and extrapolated curves, curves of friction factor vs. Reynolds number for constant Hartmann number have been plotted in Figure X. These curves are for smooth pipe flow and are in the form normally used by hydraulic engineers.

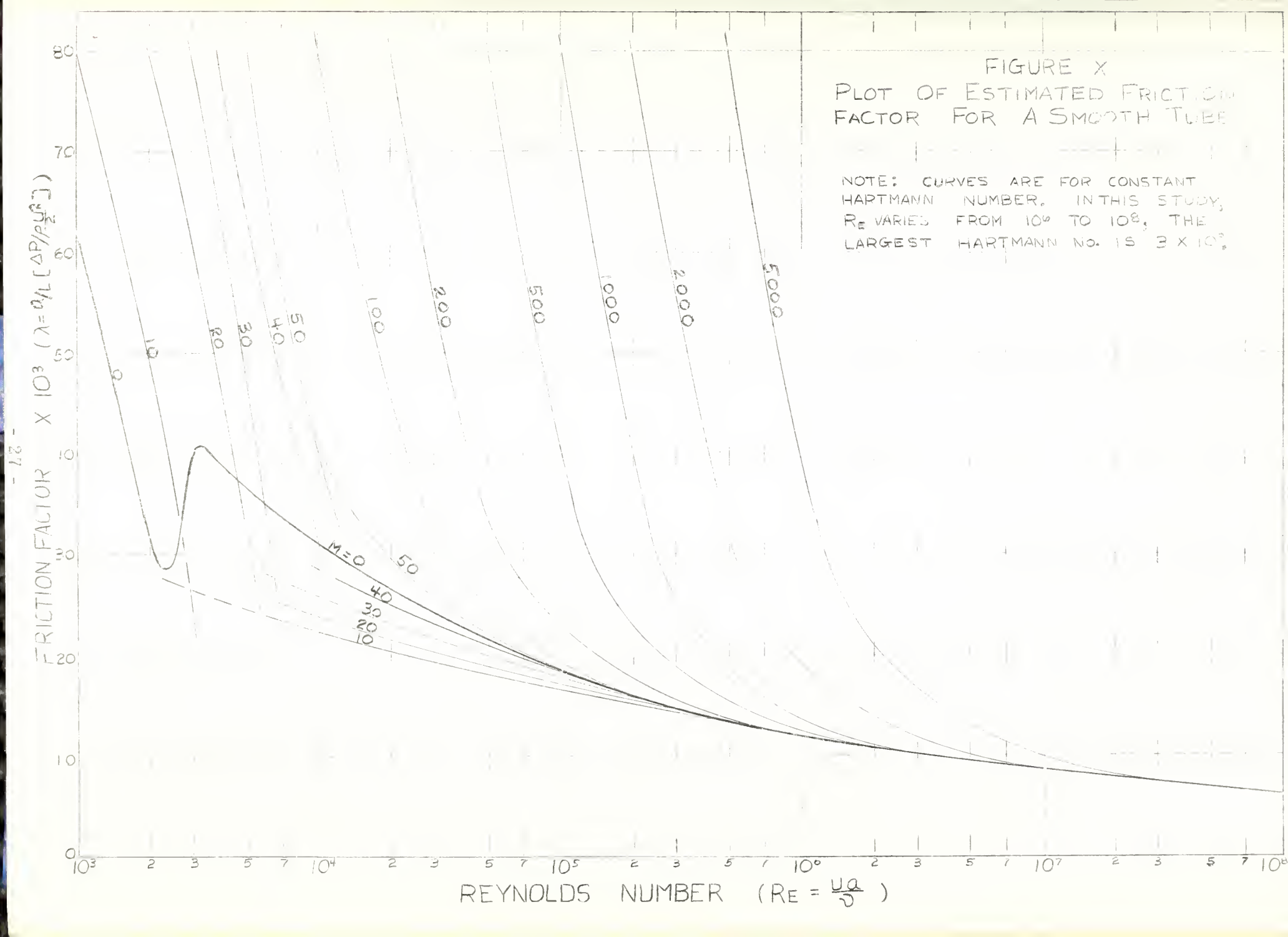
FIGURE X
PLOT OF ESTIMATED FRICTION FACTOR FOR A SMOOTH TUBE
NOTE: CURVES ARE FOR CONSTANT HARTMANN NUMBER. IN THIS STUDY, R_E VARIES FROM 10^4 TO 10^8, THE LARGEST HARTMANN NO. IS 3×10^3.
FRICTION FACTOR $\times 10^3$ ($\lambda = \tau_w / \frac{1}{2}\rho U^2$)
REYNOLDS NUMBER ($R_E = \frac{Ua}{\nu}$)
M=0
10
20
30
40
50
0
1
80
30
40
50
100
200
500
1000
2000
5000
10^3
10^4
10^5
10^6
10^7
10^8
0
10
20
30
50
70
80

III. Direct Current MHD Pump Analysis

3.1 Introduction

The engineer today is familiar with many devices in which an electric or magnetic field interacts with mechanical motion to convert energy. Electric motors and generators are perhaps the most important and well understood examples of such devices. A magnetohydrodynamic pump is essentially an electrical motor because the equations which describe its motion are exactly the same as those used to describe the motion of ordinary electric motors. The major difference is that a conducting fluid is substituted for the rigid conductor in the magnetohydrodynamic pump. The following analysis is presented in order to develop an understanding of this type of energy converter.

3.2 Mechanical Equations of Motion

If matter with an electrical charge moves through an electromagnetic field, an observer would note that the matter is acted upon by the experimentally verified Lorentz force:

$$\bar{F} = q(\bar{E} + \bar{u}X\bar{B})$$

or

$$\bar{f} = \rho_f(\bar{E} + \bar{u}X\bar{B})$$

This is the coupling force between a mechanical and an electromagnetic system. To put this more formally; the equations which completely describe a fluid-mechanical system are the equations of state and conservation of mass, momentum, and energy:

Equation of State: $\rho = \rho(p, T)$

Conservation of Mass: $$-\frac{\partial \rho}{\partial t} = \bar{\nabla}\cdot(\rho \bar{u}) \qquad [7]$$

Conservation of Momentum:

$$\rho\left[\frac{\partial \bar{u}}{\partial t} + (\bar{u}\cdot\bar{\nabla})\bar{u}\right] = -\bar{\nabla}(p + \phi) + \eta\left[\nabla^2 \bar{u} + \frac{1}{3}(\bar{\nabla}\cdot\bar{u})\right] + \bar{f}_e$$

Conservation of Energy:

$$\rho\left[\frac{\partial h}{dt} + (\bar{u}\,.\,\bar{\nabla})h\right] - \left[\frac{\partial p}{dt} + (\bar{u}\,.\,\bar{\nabla})p\right] = \frac{\bar{J}\,.\,\bar{J}}{\sigma} + \bar{\nabla}.\,K\bar{\nabla}T + \Phi$$

where:

$\bar{J}.\bar{J}/\sigma$ = ohmic dissipation

$\bar{\nabla}.K\bar{\nabla}T$ = thermal energy conduction

Φ = viscous dissipation

Note that electromagnetic coupling is evident in both the momentum and energy equations.

3.3 Electrical Equations of Motion

Maxwell's equations along with the constituent relationship for conduction current completely describe the electromagnetic system: *)

$$\bar{\nabla} \times \bar{E} = \frac{\partial \bar{B}}{\partial t}$$

$$\bar{\nabla} \times \bar{B} = \mu_o \epsilon_o \frac{\partial \bar{E}}{\partial t} + \mu_o \bar{J}_f$$

$$\bar{\nabla}\,.\,\bar{E} = \rho_f/\epsilon_o$$

$$\bar{\nabla}\,.\,\bar{B} = o$$

$$\bar{\nabla}\,.\,\bar{J}_f = \frac{\partial \rho_f}{\partial t}$$

$$\bar{J}_f = \rho_f \bar{u}_f \qquad [8]$$

Note that the electromagnetic coupling occurs specifically in the conduction current [8].

3.4 Origins of Coupling Forces

In order to arrive at an understanding of the coupling between Maxwell's equations and the mechanical equations, it is necessary to make two assumptions:

---

*) These equations, in this form, ignore polarization and magnetization which are of no importance in the device under consideration.

(a) A force is independent of the reference frame of the observer.

(b) An electrical charge is independent of the reference frame of the observer.

If two reference frames are specified, one fixed with respect to an observer, the other moving, the force on an electric charge as measured by the observer is:

$$\bar{F} = q\,\bar{E} + q\,\bar{u} \times \bar{B}$$

To another observer in the moving reference frame this force is: *)

$$\bar{F}' = q'\bar{E}'$$

since to him, the charges are stationary. Now with the assumptions (a, and b) above, this can mean only that:

$$\bar{E}' = \bar{E} + \bar{u} \times \bar{B}$$

If this same procedure is performed allowing the charge to move with respect to the moving reference frame, it can be shown that: **)

$$\bar{B}' = \bar{B}$$

This coupling between the mechanical equations and Maxwell's equations, then, can be reduced to the fact that the electrical field existing in a moving fluid is different from that applied to the fluid. In electrical motors this phenomenon is referred to as back emf and is not difficult to understand and measure.

Since, $\bar{J}' = \rho_f' \bar{u}_f' = \rho_f \left[\bar{u}_f - \bar{u}\right]$

$$\bar{J}' = \bar{J} - \rho_f \bar{u} = \sigma \bar{E}'$$

$$\bar{J} = \rho_f \bar{u} + \sigma\left[\bar{E} + \bar{u} \times \bar{B}\right]$$

Returning to the mechanical equations:

---

*) The primed variables indicate quantities as measured in the moving reference frame.

**) The above derivations are inaccurate for relativistic speed of the moving reference frame. For a derivation which includes these effects see (20).

$$\bar{f}_e = \rho_f \bar{E} + \rho_f (\bar{u} \times \bar{B}) = \rho_f \bar{E} + \bar{J} \times \bar{B}$$

3.5 Assumptions and Simplifications

All the necessary relationships have been described, but the equations are so intricate that a solution to them would be of little physical significance (if even possible). Therefore, in order to give them significance for this study the following assumptions are made:

(a) ρ = constant since sea water is relatively incompressible.

(b) ρ_f is negligible since if free charge did exist in sea water it would rapidly decay. *)

(c) $\frac{\partial}{\partial t} = 0$ since only steady state performance is of immediate interest.

(d) The effects of gravity can be ignored because of the small height variations considered.

These assumptions reduce all equations that need to be considered to: **)

$$\bar{\nabla} \cdot \bar{u} = o \quad ***)$$

$$\rho (\bar{u} \cdot \bar{\nabla}) \bar{u} = -\bar{\nabla} p + \eta \nabla^2 \bar{u} + \bar{J} \times \bar{B} \qquad [9]$$

$$\bar{\nabla} \times \bar{E} = o$$

$$\bar{\nabla} \times \bar{B} = \mu_o \bar{J}$$

$$\bar{\nabla} \cdot \bar{B} = o$$

$$\bar{J} = \sigma (\bar{E} + \bar{u} \times \bar{B}) \qquad [10]$$

3.6 Pump Efficiency

If equation [9] is dotted with u and integrated over the volume of the device the net mechanical power out is:

---

*) $\rho_f = -\frac{\epsilon_o}{\sigma} \frac{\partial \rho_f}{\partial t}$ or $\rho_f = \rho_{f_i} e^{-\frac{\sigma}{\epsilon_o} t}$ where ρ_{f_i} = initial charge, but $\frac{\epsilon_o}{\sigma} \approx \frac{10^{-9}}{(36\pi)(4)} \approx 2.3 \times 10^{-12}$ sec.

**) Since there are only two unknowns in the mechanical equations, the energy relationship is not needed.

***) Since equation [7] reduces to $\bar{\nabla} \cdot (\rho \bar{u}) = o = \rho (\bar{\nabla} \cdot \bar{u}) + (\bar{u} \cdot \bar{\nabla}) \rho$ and $(\bar{u} \cdot \bar{\nabla}) \rho = o$ because of assumption (a) above.

$$\int_{vol} \bar{u}.(\bar{u}.\bar{\nabla})\bar{u} + \bar{\nabla} p) d_{vol}$$

which is equal to: *)

$$\int_{vol} \eta \bar{u}.\nabla^2 \bar{u} + \bar{u}.(\bar{J} \times \bar{B}) \quad d_{vol.}$$

The net electrical power density into the device is:

$$-\bar{\nabla}.(\bar{E} \times \frac{\bar{B}}{\mu_o}) = -\frac{\bar{B}}{\mu_o}.(\bar{\nabla} \times \bar{E}) + \bar{E}.(\bar{\nabla} \times \frac{\bar{B}}{\mu_o})$$

$$= -\frac{\partial}{\partial t}(\frac{B^2}{2\mu_o}) \text{ **)} + \bar{E}.\bar{J}$$

which when integrated over the volume is:

$$\int_{vol} \bar{E}.\bar{J}\, d_{vol} = \int_{vol} (\frac{\bar{J}.\bar{J}}{\sigma} + \bar{u}.(\bar{J} \times \bar{B}))\, d_{vol.}$$

Therefore the efficiency of the device is:

$$\epsilon_{EL} = \int_{vol} \frac{\bar{u}.[(\bar{u}.\bar{\nabla})\bar{u} + \bar{\nabla} p]}{\bar{E}.\bar{J}}\, d_{vol}$$

It is clear that the variation of J with cross-section and length must be known before the efficiency of this device can be evaluated. From [10], J is dependent on the variation of the velocity profile even if E and B are constrained to be uniform in the cross-section. Chapter II shows that this profile is not known and therefore the efficiency of this device can only be approximated.

The hydraulics engineer often approximates the effect of velocity profile in turbulent flow by use of average velocity and multiplicative constants which are functions of the same parameters as the velocity profile. Such a procedure is applicable in this case and is presented below without the deleterious effects

---

*) It is necessary to note that $\eta \bar{u}.\nabla^2 \bar{u}$ will actually be negative and therefore be a degrading influence on $\bar{u}.(\bar{J} \times \bar{B})$ which is the power output in the absence of viscosity.

**) $\frac{\partial}{\partial t}(\frac{B^2}{2\mu_o})$ is equal to the rate of increase of magnetic energy density and equals zero for the problem.

of viscosity to show the principle variables: *)

$$\delta < J > \frac{\sigma}{w} \left[V - U B_o \right]$$

The body force applied to the fluid is:

$$\bar{J} \times \bar{B} = \delta < J > B_o$$

Therefore the power applied to the fluid is:

$$\delta U < J > B_o$$

The power applied to the electrodes is:

$$\frac{\delta < J > V}{w} = \delta^2 \frac{< J >^2}{\sigma} + \delta U < J > B_o$$

$$\epsilon_{EL} = \frac{\delta U < J > B_o}{\frac{\delta^2 < J >^2}{\sigma} + \delta U < J > B_o}$$

$$= \frac{1}{1 + \frac{\delta < J >}{\sigma U B_o}}$$

this can also be expressed as:

$$\epsilon_{EL} = \frac{U B_o W}{\frac{\delta < J > W}{\sigma} + U B_o W} = \frac{U B_o W}{V} = \frac{\text{Back EMF}}{V}$$

This simple analysis is important because it shows the extreme importance of three parameters, σ, B, and U. In general, for effective energy conversion all three should be as large as possible. Because of the hydrodynamic losses associated with large U's and the relatively fixed value of σ, the parameter of most interest is B. In this study it will be assumed that various values of magnetic field intensity are available. This point will be discussed further in Chapter VI.

---

*) It is assumed that $\bar{U}$, $\bar{B}$, $\bar{E}$, $\bar{J}$ are oriented as this:

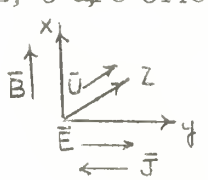

3.7 A Note on Other Effects

There are four effects associated with MHD energy conversion that have not been discussed because they are not applicable to this study, but are mentioned here for completeness and to show that high conductivities are not as desirable as some believe (1, 2):

(a) Thermal conduction losses are a problem with some MHD devices because large temperature gradients are involved. It is important here to note that the Wiedemann-Franz ratio states that the ratio of thermal conductivity to electrical conductivity is a constant with temperature. Therefore high electrical conductivity means high thermal conduction losses.

(b) Fluid current induced magnetic fields can have a serious effect on the applied magnetic field. This coupling is given by $\mu_o \bar{J} = \bar{\nabla} x \bar{B}$. Chapter II has shown that this coupling depends on Rm. For sea water and reasonable velocities and sizes this is about 10^{-4}, but for good conductors this would be 10^{2}. At the latter value induced fields would begin to be an important effect.

(c) End losses because of fringing fields and currents can have a serious effect. Sutton (19) shows that end losses are a function of magnetic field decay at the ends of the channel and the ratio of electrode spacing to channel length. If this ratio is one, the effect would be serious, but as this ratio increases this effect decreases in importance. For this study, this ratio will be approximately ten or larger and therefore will affect the overall efficiency only slightly. In this study this effect will be neglected.

(d) The Hall Effect, which is essentially an anisotropy in electrical conductivity caused by the presence of a magnetic field, can cause currents perpendicular to the load current which will increase the losses in a MHD device. The magnitude of this effect can be estimated from the cyclotron frequency and collision frequency of the charge carriers. If the ratio w_c/ν_c is of the order of one or more, this effect is important. The collision frequency is a function of the effective cross-section of the charge carrier and its target. Because of the small differences in sizes of atoms, this parameter has a relatively

small variation. The cyclotron frequency is $\frac{B}{m} \times 5.35 \times 10^{-28}$ for singly charged carriers. For an electron in a field of one weber/square meter $w_c = 6 \times 10^2$. This has been shown to be large enough to begin to be important at high temperatures. In an electrolyte, such as sea water, the charge carriers are the chlorine, sodium, hydrogen, and hydroxide ions. Each of these has a mass 10^5 to 10^6 times larger than an electron; in addition, the collision cross-section of these ions is approximately only twice that of the electron. Therefore, it is certain that the Hall Effect will not be important for this study.

IV. Procedure

4.1 The Problem Sections

When considered from the point of view, "What does it do?", the propulsion system to be studied is really a pump-jet. For this reason, the study of the system is broken into two basic parts: the hydraulic section and the electrical section. The hydraulic section consists of all those considerations which have to do with propulsion of a marine vehicle by means of a pump-jet, and specifically disregards the pumping mechanism. The electrical section consists of all those considerations which have to do with the pumping mechanism.

The hydraulic section can be broken into two parts: determination of hull and appendage drag, and the pump-jet analysis. The determination of the hull and appendage drag requires a determination of the basic hull form, control appendage drag, scoop drag, and "thrust deduction". The pump-jet analysis requires a determination of hydraulic head available at the scoop, head losses in the pump-jet duct, and the head that the pump must supply.

The electrical section considers the electrical parameters of sea water and the electrical power that must be supplied to generate the necessary hydraulic head. This section assumes the availability of uniform magnetic fields of specific intensities and electrical power source of the proper voltage and impedance levels.

4.2 Hull and Appendage Drag

The most important parameter in determining hull form and drag of a submarine is that of submerged displacement. Arentzen and Mandel state (2) "Size has been a considerable fetish with submariners ... Whereas surface ship sailors associate maximum performance with large ships ... , (the submariner)... has been accustomed to small ships which they have customarily operated out of small relatively shallow-water ports." There are many people who would like to see very small attack submarines for many well-placed reasons, but

the equipment an attack submarine must carry and the maneuverability it should possess in all directions, legislate against small ships. As a sort of optimistically reasonable size, this study uses a submerged displacement of two thousand tons.

Using reasonable parameters as indicated by Arentzen and Mandel (22) the following principle dimensions were choosen:

Length - - - - - - - - - - - - - - -	210 feet
Maximum diameter - - - - - - - -	30 feet
Prismatic Coefficient - - - - - - -	0.60

Using the methods of reference (23) and the relative drag data of Arentzen and Mandel, the basic hull and control appendage drags of Table I were calculated.

4.3 Scoop Drag

Although scoops have been used on many forms of transportation, there is very little known about them from an analytical point of view. Experimentally, many types of scoops have been tested and their drags calculated, but these have been tests of a specific scoop for a particular application. Almost always, the point of view has been, "Will this particular arrangement provide the necessary flow?" Therefore, there is no series of tests that can be used to find an optimum scoop at this time. A reasonable approach to this problem is available though, so that estimates can be made.

Hoerner (24) has shown that the total external drag coefficient of an engine installation housed in a streamline nacelle is only slightly affected by the flow rate through the ducted body where compressibility is not an important effect. These data are shown in Figure XIa.

Prior and Hall (25) examined four configerations for an air intake installed in a fighter aircraft and found that there is no change in gross drag for a nose intake, and that there is a fifteen percent increase in gross drag for side in-

TABLE I

Hull and Appendage Drag

Length 210 feet
$L_{/D}$ Ratio 7.0
Prismatic coeff. 0.60

$\Delta C_f = .004$
Displacement = 2000 tons

Speed (kts)	EHP	Thrust (pounds)
5	47	3,070
20	2,590	41,120
30	8,800	95,700
50	37,300	243,000
100	275,000	896,000

FIGURE XIA

Total Drag of Engine Installation in a Streamline Nacelle

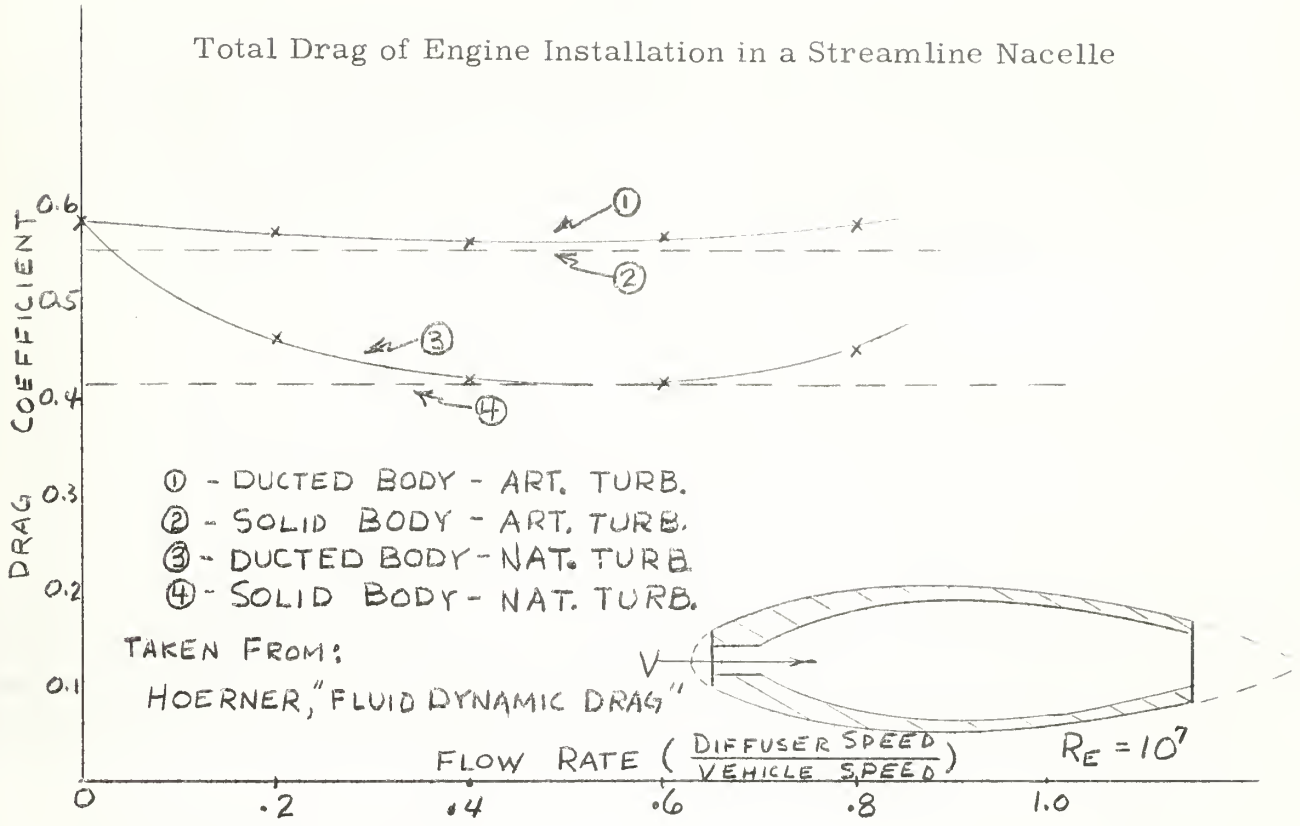

FIGURE XIB

Variation in Gross Drag for Side and Nose Intake on a Fighter Aircraft

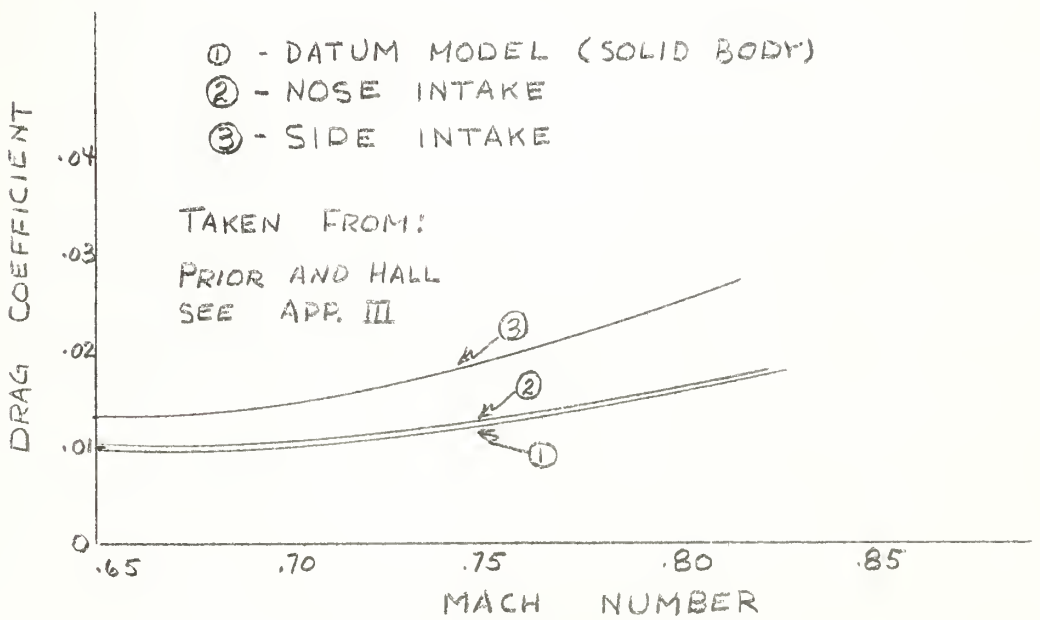

takes. In this case, the intake area was forty-two percent of the maximum cross-section of the datum model. These data are shown in figure XIb. It is encouraging to note that the predictions of Hoerner, and Prior and Hall agree for a nose intake type of scoop.

The maximum cross-section of the submarine in this study is 700 square feet; if the scoop were forty-two percent of this in cross-section it would be 300 square feet. Certainly this size of scoop is an upper limit on what could be considered feasible and is probably three to four times larger than any scoop that would be used in an actual design. Therefore, a fifteen percent increase in drag is the upper limit of the effect of a scoop.

Another method of estimating the effects of a scoop is to examine the surface area it adds to the hull, because as Arentzen and Mandel (22) describe, it is the skin friction drag that is the predominant drag on a modern submarine. If a scoop had a maximum protrusion into the flow around the hull of six feet, and it was then faired into the hull such that the form aft of the entrance of the fair-water is elliptical as opposed to circular, and this elliptical form occured over fifty percent of the hull, the increase in area would be approximately five percent. This is then a lower limit on the added drag of the scoops under consideration. For the purposes of this study, the basic hull drag with appendages has been increased by ten percent to allow for the added drag of the scoop.

4.4 Thrust Deduction

Normally, when the pressure distribution is measured around a hull, three regions are placed in evidence. First, a region forward of amidship where the pressure is above ambient and therefore tends to retard the motion of the hull. Second, a region centered about amidship where the pressure is below ambient and, because of the slope of the hull in this region, is of minor importance in relation to the forces on the hull. Third, a region aft of amidship where the pressure is above ambient and therefore tends to aid the motion of the hull. When a propeller is placed at the stern of a hull, a pressure difference exists

across the blades of the propeller. The pressure on the side towards the hull is lower than ambient and therefore detracts from the assisting action of the undisturbed pressure field. This decrease in pressure or increase in drag is called thrust deduction and is of considerable importance in the design of a hull.

When a pump-jet device is used to propell a hull, the pressure at the nozzle exit of the duct can be designed to match that of the undisturbed pressure field. This means that the position of the entrance to the diffuser will determine any thrust deduction because of a change in pressure field. Because of the pumping action of the device, the pressure at the entrance will always be below ambient. Therefore, if the entrance is at a portion of the hull parallel to the direction of motion there will be no force in the direction of motion and therefore, no thrust deduction. If the entrance is at a portion of the hull at an angle to the direction of motion, this reduced pressure can act as either a thrust deduction or a thrust addition. Figure XII shows a typical pressure difference plot and the effects of various locations of the scoop entrance. Clearly, it is a problem of design where the entrance should be, since the length of the duct is a factor in the added surface area of the scoop and its internal losses. This problem is most readily solved by model testing procedures and is beyond the scope of this study. The point that is clear, is that there need not be a thrust deduction when using a pump-jet device and therefore none will be used in this study.

4.5 The Pump-Jet Analysis

The pump-jet must produce enough thrust to overcome the hull and appendage drag. Since pressures exterior to the duct are considered to be a component of hull drag through the use of thrust deduction, this drag must be overcome solely by means of an increase in momentum of the fluid flowing through the device. In other words, the pump-jet takes fluid with a certain velocity head; adds the necessary amount of pressure head; then converts this to velocity head in a nozzle such that the difference between exit and entrance momentum

FIGURE XII

The Pressure Variations Accounted for by Thrust Deduction

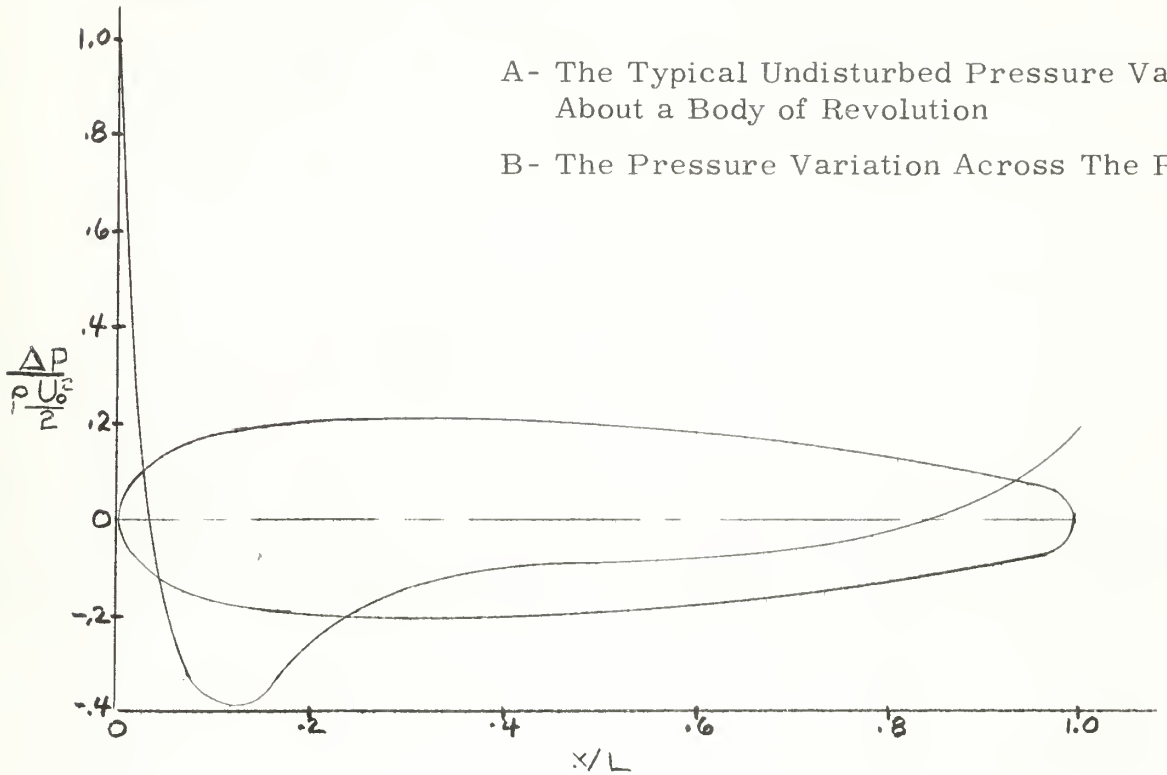

A- The Typical Undisturbed Pressure Variation About a Body of Revolution

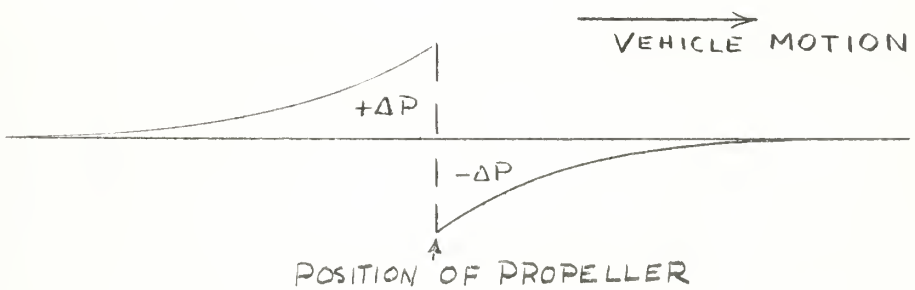

B- The Pressure Variation Across The Propeller

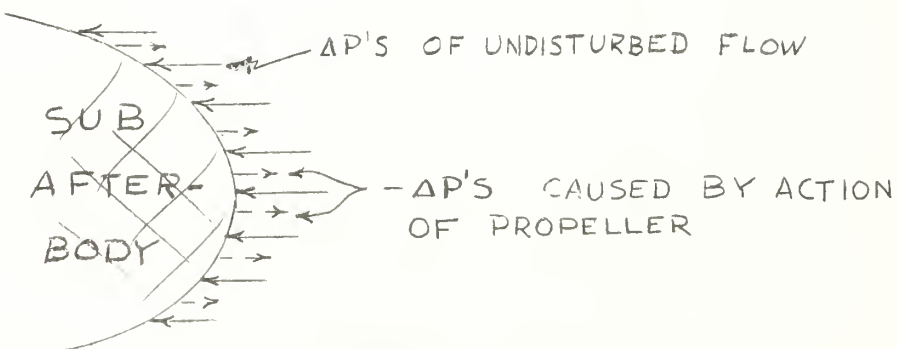

equals hull drag. Therefore, using the nomenclature of Figure II:

$$T = \rho A_2 U_2^2 - \rho A_1 U_1^2$$

Continuity of mass requires that:

$$A_0 U_0 = A_1 U_1 = A_2 U_2 = Q$$

$$\rho = \text{constant}$$

Therefore:

$$T = \rho A_1 U_1 (U_2 - U_1) = \rho Q (U_2 - U_1)$$

From an energy point of view:

$$\left[\frac{U_0^2}{2g} + \frac{p_0}{} + Z_0\right] \gamma Q = \left[\frac{U_1^2}{2g} + \frac{p_1}{} + H_{L_{0-1}} + Z_1\right] \gamma Q$$

$$\left[\frac{U_1^2}{2g} + \frac{p_1}{} + Z_1\right] \gamma Q = \left[\frac{U_2^2}{2g} + \frac{p_2}{} + H_{L_{1-2}} + Z_2 - H_p\right] \gamma Q$$

since: γQ = constant

$$H_p = \frac{U_2^2 - U_0^2}{2g} + \frac{p_2 - p_0}{} + Z_2 - Z_0 + H_{L_{1-2}} + H_{L_{0-1}}$$

The efficiency of this section is defined as hydraulic efficiency:

$$\epsilon_H = \frac{T V_0}{\gamma Q H_p}$$

The foregoing analysis is accurate for uniform velocity. If there is any variation of the velocity profile with cross-section the momentum equation becomes:

$$T = \rho \int \left[u_2 - u_1\right] dQ$$

where u = f(A)

The momentum equation may be written in terms of the mean velocity of each section together with a coefficient β such that:

$$T = \left[\beta Q \rho U\right]_2 - \left[\beta Q \rho U\right]_1$$

$$\beta = \frac{1}{Q} \int \frac{u(A)}{U} dQ = \frac{1}{A} \int \left(\frac{u(A)}{U}\right)^2 dA$$

A u(A) $\neq$ constant also requires a correction to the energy analysis:

Kinetic Energy at section $= \frac{\alpha U^2 Q}{2g}$

in which $\alpha = \frac{1}{Q}\int \left(\frac{u(A)}{U}\right)^2 dQ = \frac{1}{A}\int \left(\frac{u(A)}{U}\right)^3 dA$

For hydrodynamic flow since u(A) is a function of roughness and Reynolds number, so are α and β. If $R_E = 10^7$ and the flow is smooth, $\alpha = 1.02$ and $\beta = 1.01$.

The head losses from 0 to 2 can be divided into four categories:

(a) Entrance Losses

(b) Diffuser Losses

(c) Channel Losses

(d) Nozzle Losses

The procedure used to approximate these losses can be found in Appendix I.

4.6 The Electrical Section

Equation [10] can be rewritten as follows using the coordinates of Figure II:

$$- \int_W \bar{E}.\, d\bar{y} = V = - |E|\, w$$

$$- \int_D \int_L \bar{J}.\, d\bar{y} = - I = - \delta \langle J \rangle D L$$

$$I = \frac{\sigma D L}{w} (V - U_z B_x w)$$

$$I R = V - U_z B_x w$$

$$R = \frac{w}{\sigma D L}$$

This equation can be represented by the following analogue:

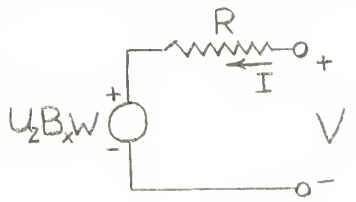

It is apparent from this that the only source of loss in the electrical section

of this device, is the $I^2 R$ loss in the fluid.*)

The power that the electrical section must produce is:

$$\text{Power out} = \rho Q H_p$$

$$\text{Power in} = I^2 R + \rho Q H_p = V I$$

Therefore, the efficiency of the electrical section is:

$$\epsilon_{EL} = \frac{\rho Q H_p}{V I}$$

The total efficiency of the device is:

$$\epsilon_{Total} = \epsilon_{EL} \epsilon_H = \frac{T V_o}{V I}$$

The above method of estimating the efficiency of an MHD pump-jet was applied to the IBM 7090 Computer at M.I.T. In these computations certain parameters were varied; these parameters and the results of these machine computations are presented in Chapter V.

---

*) See Section 3.7 for a note on other electrical effects.

V. Results and Discussion

5.1 Definition of Terms

Using the procedure of Chapter IV, channel voltage, current density, various losses, hydraulic efficiency, electrical efficiency, and total efficiency of a MHD pump-jet, used as the main propulsion for a two thousand ton submarine, with the variation of several parameters, were calculated. The parameters which were varied and their definitions are as follows:

(a) Speed of vehicle. This variation is discussed in section 4.2 and the specific data are presented in Table I.

(b) Geometry of pump-jet.

1. Cross-section area. This is the area at section C in Figure II.
2. Diffuser ratio. The area ratio Ac/A_1.
3. Jet ratio. The area ratio A_c/A_2 .
4. Channel length. The length of the constant area section, i.e. section C-C.

(c) Inlet Speed. Bulk average flow into pump-jet at section 1.

(d) Magnetic Flux Density. Strength of field across channel, field is assumed to be uniform over entire length of channel.

In these calculations the following conditions were assumed:

(a) The channel cross-section is square. Aspect ratios up to three were calculated, but all effects on efficiency were minor.

(b) Thrust deduction accounts for all pressure distributions in their entirety. For this study, the variation of thrust deduction with speed and other conditions (e.g. inlet speed) is assumed negligible.

(c) The bulk average at the exit of the jet nozzle must exceed the vehicle speed.

(d) The conductivity of sea-water is 4 mhos/meter.

All the data which were used to plot the following curves can be found in Appendix II.

5.2 Variation of Efficiencies With Vehicle Speed

Figures XIV through XVIII collectively show the variation of electrical and total efficiency with speed.

Because the required pumping power is a function of speed and hydraulic efficiency, and the hydraulic losses increase with the bulk velocity squared, it is to be expected that current densities must be proportionally higher for higher speeds. This fact, coupled with the increase in back emf with speed, requires more electrical power to be added to the MHD pump as speed is increased. Therefore, as shown in Figures XIV through XVIII, for constant power output, fixed geometry and magnetic flux density, both electrical and total efficiency decrease with speed. The faster change with speed of total efficiency as compared to electrical efficiency also shows that hydraulic efficiency is decreasing.

5.3 Variation of Efficiencies With Channel Geometry

The variation of electrical, hydraulic, and total efficiency with length and channel area is shown in Figure XIII.

Figures XIV and XV show the effect of diffuser ratio and jet ratio on electrical and total efficiencies.

Hydraulic losses are surface losses; therefore, an optimum volume is the one which has the lowest surface to volume ratio ($S/\sqrt[3]{Vol^2}$). For this reason, the hydraulic efficiencies favor the shorter lengths with the largest channel cross-sections.

The electrical losses are volume losses and therefore, by themselves, do not have a preferred geometry. Because in this study, the current densities are controlled by the pump head necessary in the pump-jet and this is a function of hydraulic losses and bulk flow rate, large volumes require the lowest current densities and therefore are the most efficient. It is important to note that in every case, the longer length channels are more efficient electrically

and less efficient hydraulically. As Figure XIII shows, these conflicting trends make channel areas of approximately one hundred square feet highly desirable almost regardless of length. Figures XIV and XV show that this area is also relatively insensitive to vehicle speed.

Normally a large diffuser ratio is considered desirable in a hydraulic energy converter because this decreases bulk velocity and the ratio of surface area to volume; both of these results decrease the fluid losses. This desirable result is modified by the need for larger jet ratios to maintain the momentum change through the pump-jet as the diffuser ratio is increased. This is not desirable because large jet ratiosimply large hydraulic losses. As previously discussed, the electrical efficiency will be improved when diffuser ratio is increased because this reduces pump head and current density. Figures XIV and XV show that:

(a) Efficiencies favor lower jet ratios.

(b) For each jet ratio there is a diffuser ratio that is best. This relationship is such that U_2 / U_1 is about 1.25 regardless of speed.

In general, it can be stated that the hydraulic losses are the controlling losses in the MHD pump-jet; therefore, any change in geometry should be made to decrease these losses. A desirable cross-section area is one hundred square feet; a desirable length is fifty feet, and the lowest jet ratio that will maintain U_2/U_1 at about 1.25 is the most efficient.

5.4 Variation of Efficiencies With Inlet Speed

Inlet speed is perhaps the most important parameter excluding magnetic flux density, but it is also the most difficult to evaluate. This difficulty occurs because reasonable geometries of the pump-jet require large flow rates and it is not possible to determine what the lowest bulk velocity is that will not seriously affect drag. As has been previously stated, hydraulic losses depend on bulk velocity squared; therefore, low velocities are highly desirable. It is to be noted that because of the shape of the boundary layer around the hull, al-

most any bulk velocity is possible, but this is not true of the combination flow rate and bulk velocity. Because no data are available on minimum velocities, no attempt has been made to estimate this other than to constrain the outlet velocity of the jet nozzle (this has the effect of setting a minimum inlet speed for reasonable geometries).

Figures XIII, XIV and XV all are based on inlet speeds equal to or greater than the vehicle speed; for these conditions it is certain that the hydraulic efficiencies, as calculated, are good estimates. These efficiencies are of the order of sixty percent. Figures XVI, XVII, and XVIII are based on inlet speeds less than eighty percent of vehicle speed and produce hydraulic efficiencies of the order of ninety percent. This variation defenitely shows the significance of this parameter. It is almost certain that efficiencies of ninety percent are not possible, and are actually a breakdown in the model used for this study. This does not detract from the fact that, in general, inlet speeds less than vehicle speed are possible and desirable.

5.5 Variation of Efficiencies With Magnetic Flux Density.

As Figures XVI, XVII, and XVIII show, the magnetic flux density has a primary beneficial effect on electrical efficiency and therefore, on total efficiency. Because the magnetic flux density can affect friction factor, as described in Chapter II, there are cases where an increase in magnetic flux density will not increase total efficiency as much as electrical efficiency. The geometries and velocities of this study are such that for the magnetic fields considered, this effect occurs only at the lowest speeds. The reasons for the increase in efficiency with magnetic field have been stated in Chapter III and will not be repeated here. It is important to note that even with fields of between five and ten webers per square meter, the total efficiency is technically interesting and it is in this variation of field density that the largest gains are made in total efficiency.

5.6 Summary

It has been shown that the geometry of the MHD pump-jet is important in so far as it affects hydraulic losses and necessary pump head, and that the optimum geometry is relatively insensitive to vehicle speed. The magnetic flux density has a primary effect on electrical efficiency because of the decrease in current densities required for constant pump head. In general, any geometry or other parameter that will decrease current density will increase the electrical and total efficiencies. With all these effects considered, the geometries and magnetic flux densities necessary to provide reasonable efficiencies at low speed are technically feasible at this time.

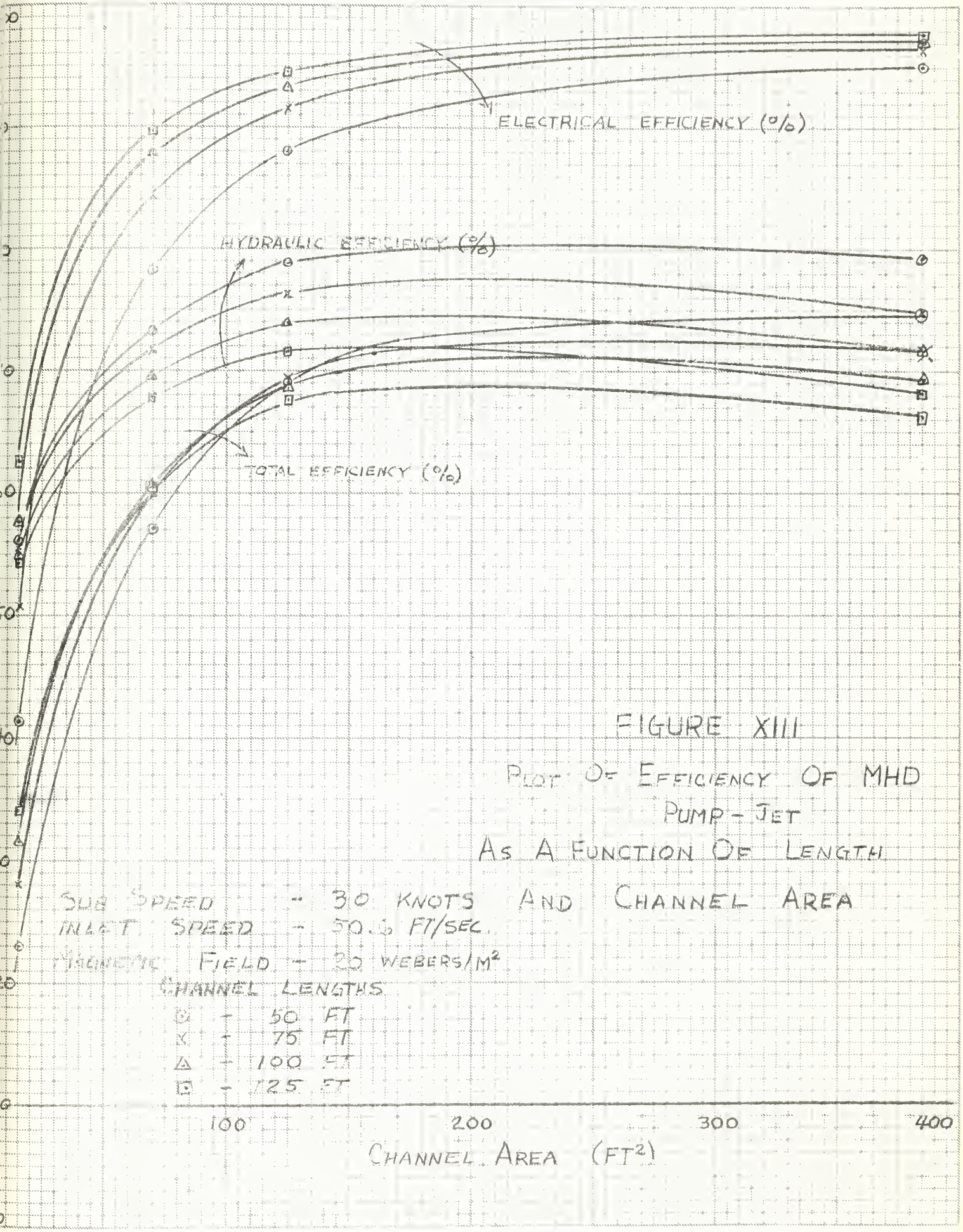

FIGURE XIII

PLOT OF EFFICIENCY OF MHD PUMP-JET AS A FUNCTION OF LENGTH AND CHANNEL AREA

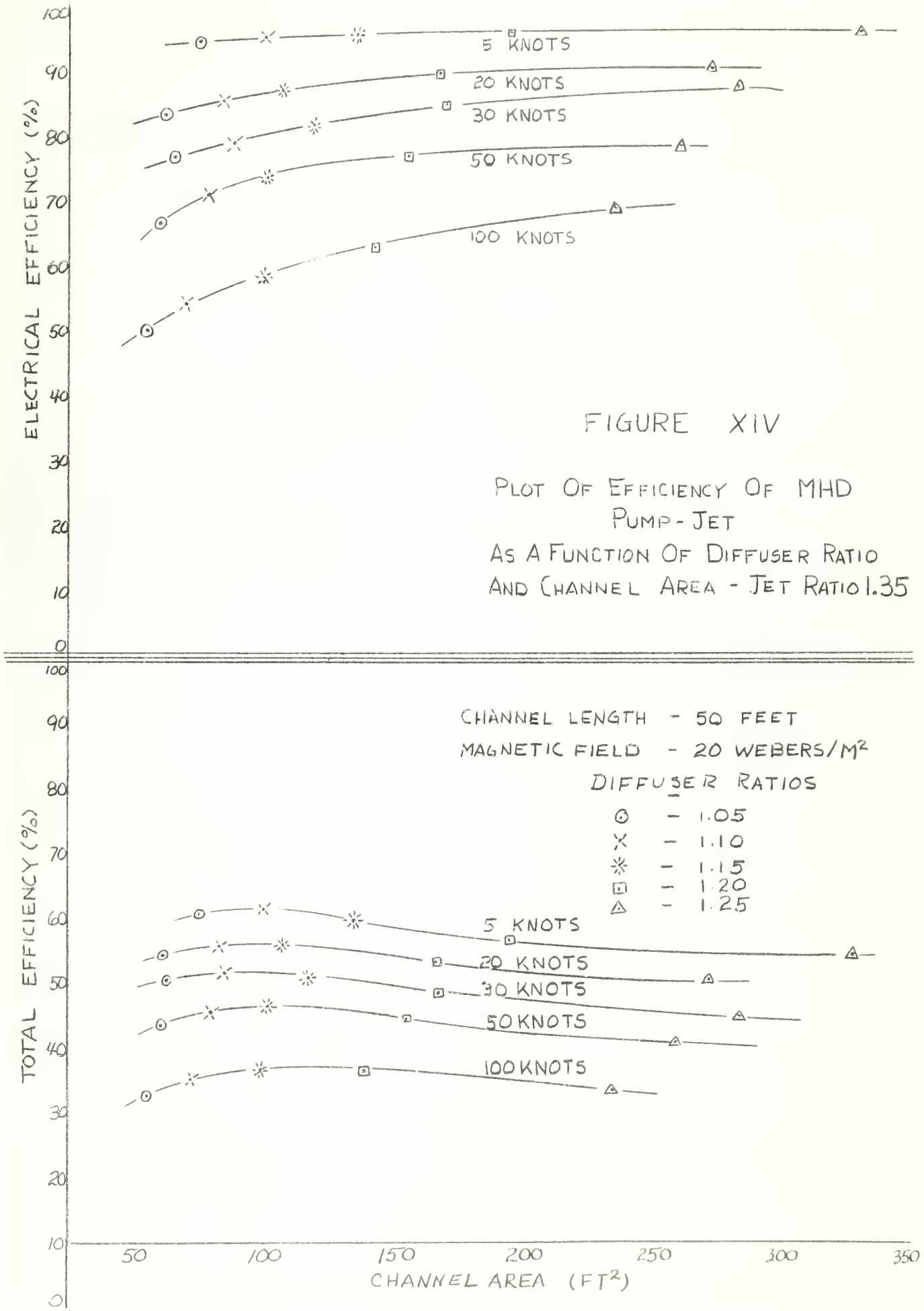

FIGURE XIV

PLOT OF EFFICIENCY OF MHD PUMP-JET AS A FUNCTION OF DIFFUSER RATIO AND CHANNEL AREA - JET RATIO 1.35

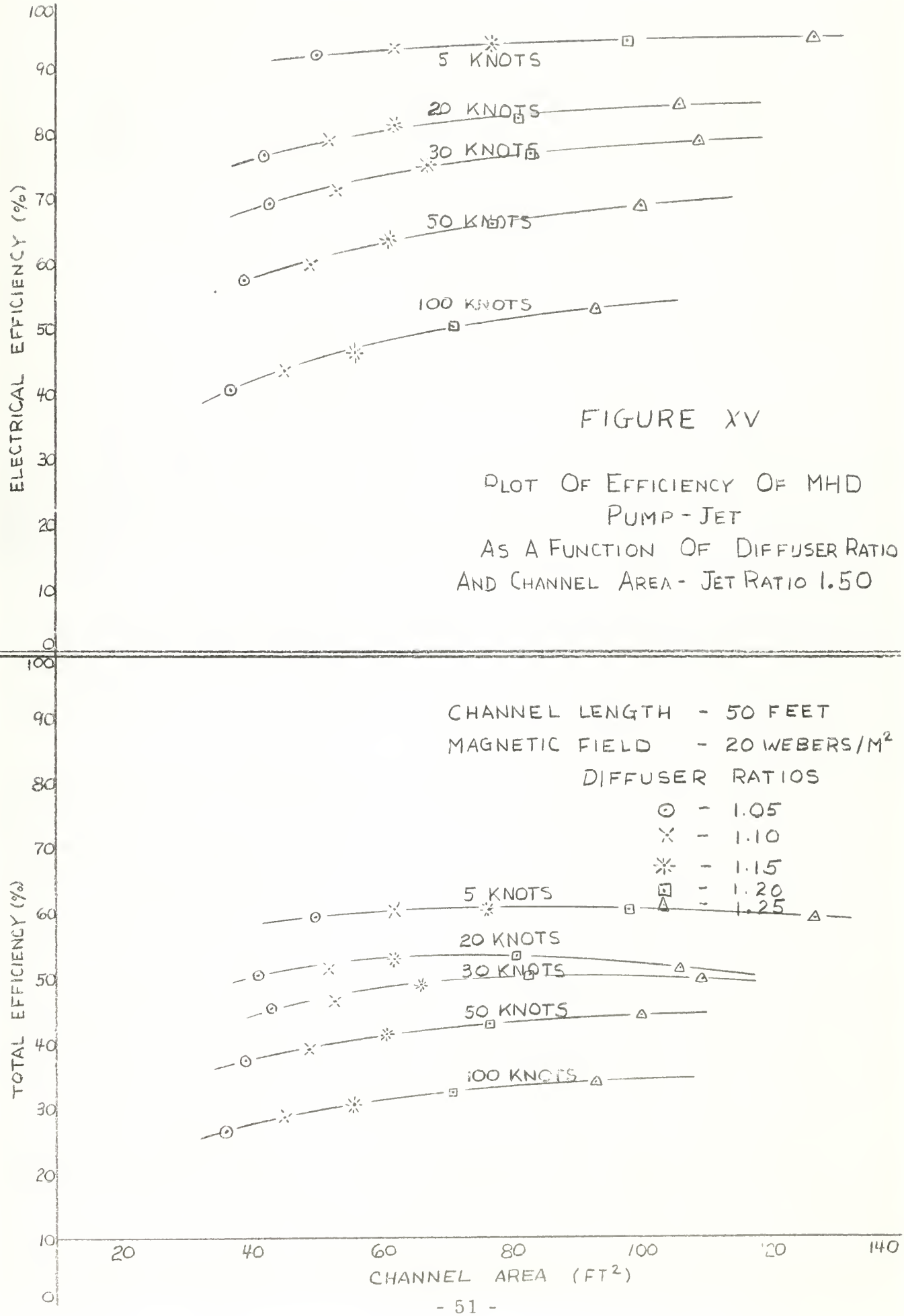

FIGURE XV

PLOT OF EFFICIENCY OF MHD PUMP-JET AS A FUNCTION OF DIFFUSER RATIO AND CHANNEL AREA - JET RATIO 1.50

FIGURE XVI

Plot of Efficiency of MHD Pump-Jet as a Function of Speed for Fixed Geometry, Channel Area 100 Square Feet.

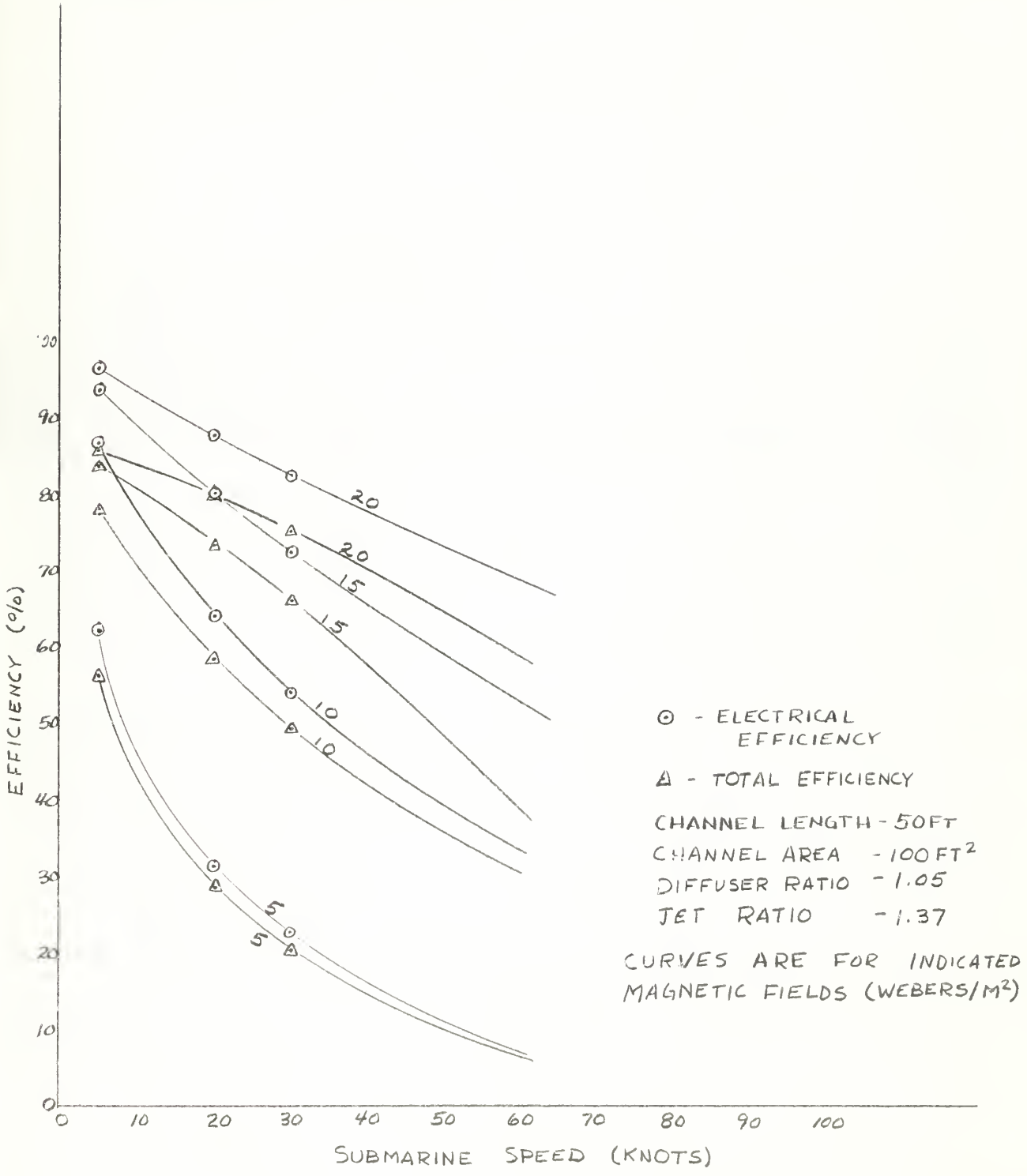

FIGURE XVII

Plot of Efficiency of MHD Pump-Jet as a Function of Speed for Fixed Geometry, Channel Area 75 Square Feet.

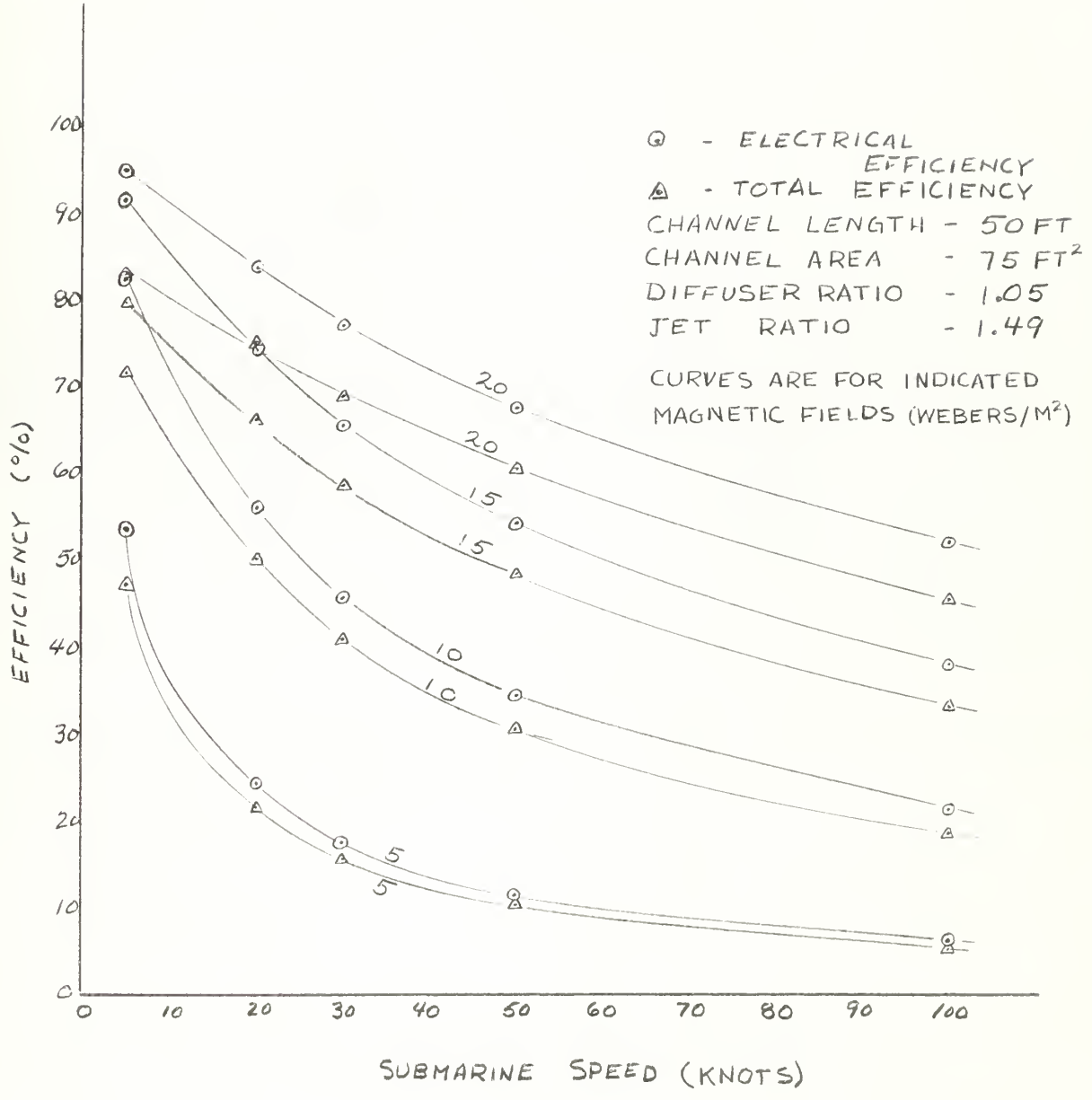

FIGURE XVIII

Plot of Efficiency of MHD Pump-Jet as a Function of Speed for Fixed Geometry, Channel Area 50 Square Feet.

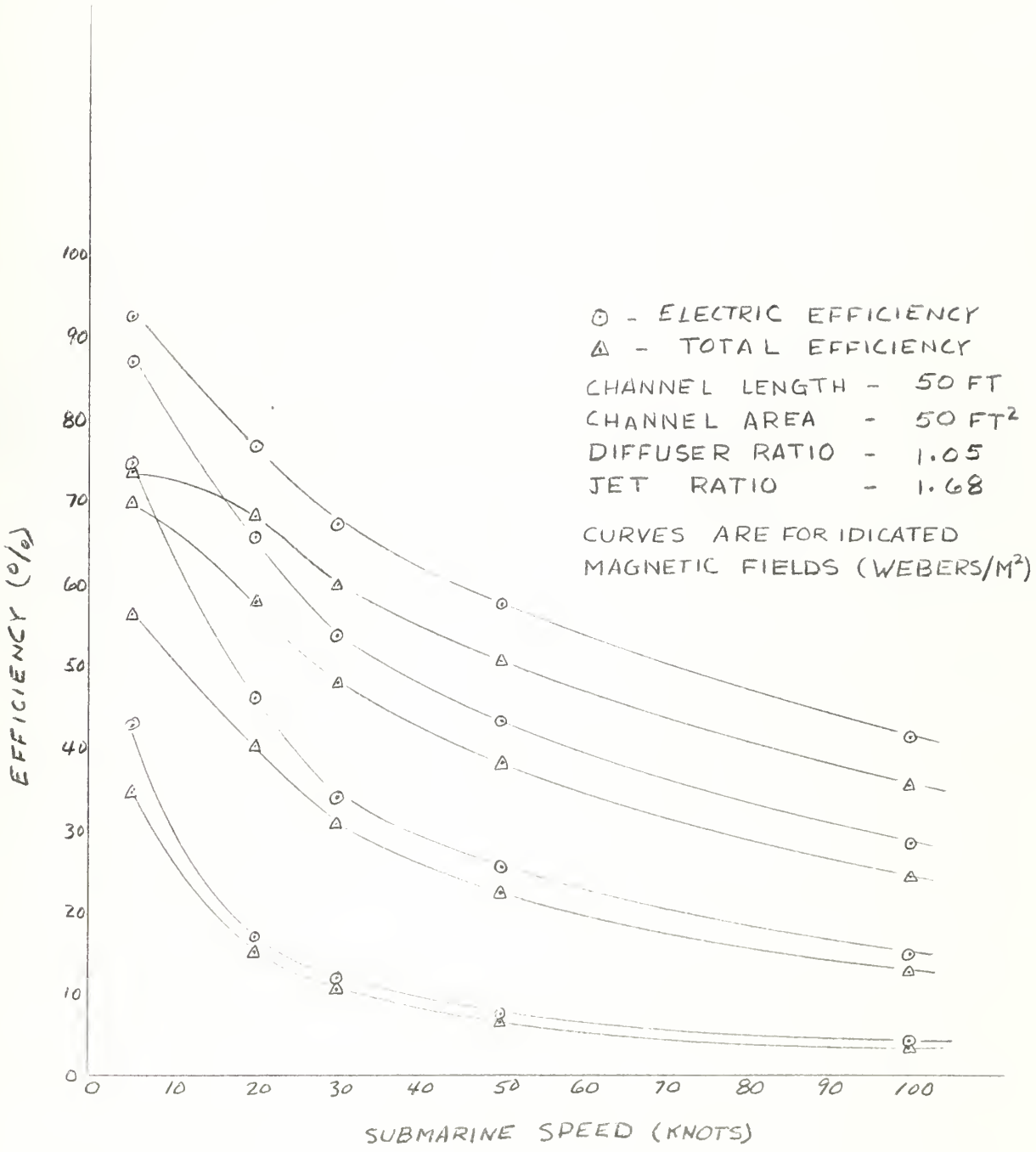

VI. Complicating Problems

6.1 Introduction

In the introduction to this study, it was stated that the objective was to study the MHD pump-jet to see if it is a possibly feasible propulsion device for a marine vehicle. Up to this point, it has been shown that it can be operated reasonably efficiently and that, in general, the device is interesting because of its compactness, noise-free operation, and ability to couple large amounts of power to water. The problems associated with these characteristics will be outlined here in order to place some of what they entail in evidence.

6.2 Noise-Free Operation

In a fluid flow process, noise sources can be divided into three types: monopole, dipole, and quadrupole. Mass and heat fluctuations act as monopoles, pressure and rigid body motions act as dipoles, and fluid turbulence acts as a quadrupole. The strength of the sound transmitted is dependent upon the power of the source and its type of transmission in the fluid. Source sound power is coupled to the fluid in ratios from 10^{-5} to 10^{-8}, it is then propagated according to its characteristic type. A monopole type propagation is proportional to the local Mach number; a dipole , to Mach number cubed; and a quadrupole, to Mach number to the fifth power.*) Since local Mach numbers are much less than one, it is obvious that a quadrupole type of propagation is far and away the most desirable.

This then is the basic advantage of a MHD pump-jet; its coupling is a fluid turbulence one as opposed to the pressure coupling of a screw propeller. As with the propeller though, this fact would become meaningless if a mass source appears as in cavitation or other bubble motion. Such a source is potentially available in the electrolysis of the sea water.

---

*) Note that in db the dipole is down 20 db from the monopole and the quadrupole is down 40 db at any comparable location.

TABLE II

Amount of Gas Formed at Electrodes of a 100 Square Foot Square MHD Channel in Sea Water.

Current Density (amps/meter^2)	Single Electrode Gas Rate (ft^3/HR)	Total Gas Rate (ft^3/HR)
50	34.3	68.6
100	68.6	137.2
200	137.2	274.4
500	343.0	686.0
1000	686.0	1372.0
5000	3430.0	6860.0
10000	6860.0	1372.0

When an electric current passes through sea water, it does so by ionic conduction. That is by actual migration of ions which bear charges of positive or negative electricity. These ions can pass only as far as the electrodes where their charges will be neutralized with the release of uncharged, electrically neutral matter. In sea water this matter will be essentially chlorine and hydrogen gas. By noting that the ion motion is directly proportional to the current flow, it is possible to calculate the amount of this gas that will be released. If these gases are not removed from the fluid, they will be swept through the varying pressure field in the pump-jet and act as a pulsating mass. Table II shows the amount of these gases that will be generated for various current densities in a one hundred square foot channel. Appendix II shows the current densities that are necessary for the various geometries and speeds as specified. At this time, it is an academic question as to the effectiveness of any method of removing these gases from the fluid. One possible method is to shield the electrodes in the channel with porous walls, and then to separate the gases from the water between the wall and the electrode. If these gases are then burned in a fuel cell, they can be converted to HCl and the resultant power used to provide the motive power for the gas removal system. It is even possible that some power will be available for other uses. There are two basic questions that must be answered in this respect:

(a) Are the gas bubbles that are formed significant enough as noise sources to make such a system necessary?

(b) Will the system, if built, be effective enough to justify its development?

6.3 Compact Propulsion System

The compactness of a MHD pump-jet is a matter of necessity for the following reasons:

(a) It is necessary to shield the magnetic field to lower the vehicle's magnetic signature.

(b) It is necessary to shield and generate the magnetic field with supercon-

ductors. The cryogenic temperatures that this implies put a premium on minimum surface area to minimize heat transfer.

(c) The shield will have to absorb the magnetic energy in the magnetic field; with ten webers per meter squared this is equivalent to sixty psi. Such pressures, over ambient are most easily absorbed in small sizes.

(d) Even if it were not militarily necessary to shield the magnetic field, it would be necessary to do so for health reasons.

The magnetic shield then provides the compactness of the propulsion system, but it also complicates the structural problem associated with this device. Because the structural problems are closely associated with the magnetic energy storage which is dependent on the specific superconductor used, it is perhaps best to start with the superconductor to develop the problem.

As described in Chapter I, all of the superconductors of interest in this problem can be divided into two groups, i.e. alloys or compounds. The alloy superconductors worked to a high degree before they retain their superconducting characteristics at relatively high magnetic fields. This deformation is the reason why ten mil wire is the standard of the industry. Even under this reduction the alloy superconductors tend to retain good ductility. The compound superconductors are brittle and difficult to shape. These differences manifest themselves when the magnetic field coil is wound and used. The alloy superconductors require tedious methods for proper winding of the ten mil wire and, when the coil is completed, it has a very large inductance because this is proportional to the number of turns squared. In addition to this, even though short samples of this material can remain superconducting in fields about five webers per square meter and carry current of 18×10^8 amps per square meter (26), wound coils seen unable to carry more than twenty percent of this.*) The compounds could conceivably be formed into coils with relatively low inductances and have a better chance of carrying larger super currents, if indeed the failing in alloy superconductors is due to "the weakest link" as some suspect (27). The size of coils is important because it will determine the size

---

*) Recently there have been indications that coils can be wound to maintain the same currents as small samples, although this has not yet appeared in the literature.

of protection devices. At normal temperatures the resistance of some superconductors is very high and if a coil should be suddenly placed in such an environment, it would be melted down if no protection devices existed.

Once a suitable superconductor has been chosen, there are still the problems of maintaining its environment and holding it together. Maintaining the environment amounts to having a cryogenic system large enough to supply the 4°K atmosphere at the expected evaporation rate. The evaporation rate is controlled by the surface area of the dewar and the methods of heat transfer. The heat transfer can be minimized by:

(a) Maintaining a vacuum in the dewar to eliminate convective losses.
(b) Using multi-layered foil in the vacuum to reduce radiation losses.
(c) Minimizing conduction losses by making all structural connections through the dewar as long and as thin as possible. This last might be called "bicycle wheel" construction.

As an indication of the size of the cryogenic plant, it should be noted that using a Carnot refrigeration cycle between 300°K and 4°K would require seventy-four units of power input for each equivalent power unit of refrigerant evaporated. If a refrigeration cycle as efficient as the normal home refrigerator were used this ratio would be 300:1 and if a presently available cryogenic cycle were used it would be 1000:1. Of course, a highly efficient multi-cycle system could be used quite conveniently aboard a submarine if the cryogenic system were used to do all refrigeration work onboard. For example, a freon cycle would be used to about 270°K and provide air conditioning and normal refrigeration; then a nitrogen cycle could be used to about 75°K and provide air regeneration and scrubbing needs; and finally a helium cycle to 4°K. It might be noted that a system of this size could also incorporate a gas storage system for blowing tanks by expansion of the gas from the liquid to the gaseous state. Such a system would require very little storage volume.

Finally, one has the structural problems. The presence of the dewar and the need for "bicycle wheel" construction have already been noted, but there

is more than this. Stekly (28) has discussed this subject; a few of the more prominent points of this discussion will be repeated here for the sake of completeness.

The energy storage per unit volume in a magnetic field is equal to $B^2 / 2\mu_a$. It is this energy that the magnetic field coil and shield must transfer to the supporting structure. Levy (29) has shown that a minimum possible structural weight results if all structure is in tension. This minimum is:

$$M_{ST} \geq \frac{\gamma_{ST}}{\sigma_w} \frac{B^2}{2\mu_o}$$

where γ_{ST} is the density of the structure, and σ_w the working stress. Stekly goes on to show that in an actual design this minimum cannot be achieved since some of the structure must be in compression; perhaps a more realistic structural weight is three times the minimum weight. This structural weight is significant and will be further complicated by the structure necessary to transmit the thrust from the pump-jet to the hull.

In summary, there are basic development problems in the fabrication of superconductors, in cryogenic systems, and in the supporting structure. There also is a question concerning noise-less operation of a MHD pump-jet, but it is important to note that although any one of these problems might eventually limit the usefulness of a MHD pump-jet, they do not, a priori, present problems which are any different than those which have been met in the development of other propulsion device.

VII. Conclusions and Recommendations

A magnetohydrodynamic pump-jet is a technically interesting means of propulsion for a marine vehicle. It has inherent compactness and could be used to produce high power at low noise levels and relatively small submarines. This small size would be the result of the lack of maintenance personnel and the size of the propulsion system. There are major development problems associated with this type of propulsion system, but none of them preclude its development at this stage.

These development problems can be summarized as follows:

(a) The study of the effect of a magnetic field on velocity and current profiles.

(b) The study of the effect on drag of pump-jet propulsion.

(c) The fabrication of a superconductor in a more easily used form than ten mil wire.

(d) The development of an efficient multi-cycle cryogenic system.

(e) The development of structure capable of supporting the magnetic field coil and shield as well as transmitting the pump-jet thrust to the hull, all with the necessary thermal limitations of a dewar.

(f) The development of an efficient gas exhaust system to insure quiet operation of the propulsion system.

The analysis of the above problem and perhaps the solution of the first two are within the normal realm of thesis topics and it is recommended that they be so treated. An entirely new type of propulsion system that offers the possible characteristic of quiet high speed operation at reasonable efficiency should easily provide the impedous necessary to study this system thoroughly.

APPENDIX I

Computational Methods and Approximations

A. Conductivity of Sea Water *)

In general, the conductivity of sea water varies with chlorinity, temperature, and geography. Chlorinity can be found from salinity since:

$$\text{Salinity} = 0.03 + 1.805 \times \text{Chlorinity}$$

The salinity varies from 33°/oo to 37°/oo over most of the ocean, but there are some exceptions such as the Gulf of Bothnia where the surface salinity is zero and the Red Sea where it is 40°/oo. The conductivity decreases quite rapidly with temperature and salinity. The temperature of the oceans are fairly predictable. The temperature of deep and bottom water is between 4° and -1°C and at the surface can be as much as 30°C.

A conductivity of four mhos/meter was used for this study; this corresponds to a temperature of 12°C and a chlorinity of 19°/oo and is approximately the conductivity of sea water in the Atlantic Ocean at about 400 feet in depth.

B. Hydraulic Loss Coefficients

There are five loss coefficients of interest in this study. These loss coefficients all fit the formulation:

$$H_L = K \frac{U^2}{2g}$$

where H_L is the head loss and U is the maximum velocity of the section in question. The coefficients and their approximations are as follows:

(a) Entrance Loss. This is a significant loss which results from the contracting of the fluid flow lines when the fluid enters a channel from a reservoir.

---

*) Reference for this data is SVERDRUP et al., The Oceans, Prentice Hall, 1942.

The maximum velocity head is based on vehicle speed, and all that is not present in the inlet velocity head is assumed loss on entrance. In addition there is a minimum entrance loss based on a bell mouth entrance which is normally assumed to be five percent of the total head. The approximations used in this study were:

$$H_L = \frac{U_o^2 - U_1^2}{2g} \qquad \text{if} \quad U_o^2 - U_1^2 > .05\ U_1^2$$

$$= \frac{.05\ U_1^2}{2g} \qquad \text{for all other cases}$$

(b) Turn Losses.*) The losses from fluid flow in a turn are dependent on the radius of the turn, the velocity distribution in the inlet, the skin friction of the pipe, and the induced secondary currents. It is necessary to avoid any velocity distribution which places the high velocity on the inner side of the bend since this can increase losses by four times the normal value. In this study bends were not assumed to be present.

(c) Diffuser Losses. These losses are caused by separation of the fluid flow lines and vary with the angle of divergence. The loss coefficient can be approximated by:

$$K = .03\ \left(\frac{A_1}{A_2} - 1\right)$$

if the angle of divergence is kept less than three degrees.

(d) Channel Losses. Chapter three has described channel friction factors. In general:

$$K = \frac{\lambda L}{D_H}$$

where:

$$\lambda = \lambda_{M=o} + 5\ M/R_E \text{ if } M/R_E > .0002$$

$$= \lambda_{M=o} \qquad \text{for all other cases}$$

(e) Nozzle Losses. These losses are due to secondary flows and skin friction and can be approximated by:

$$K = \left(\frac{1}{(.98)^2} - 1\right) \left[1 - \left(\frac{D_2}{D_1}\right)^4\right]$$

---

*) Yarnell, D. L., and Hagler, F. A., Trans. Am. Soc. Civil Engineers, 1935, pp. 1018 - 1032.

C. Logic Flow of Computer Program.

A FORTRAN computer program was written in order to study the MHD pump-jet previously described. The logic used in the solution is shown in Figure XIX.

The following symbols are used in the diagram:

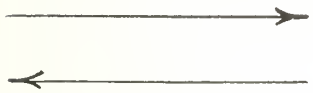

Direction of Flow

Program Step

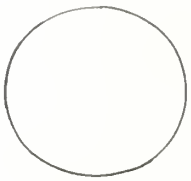

Stop

Input/Output

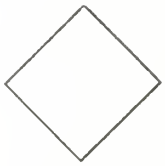

Decision

Some of the results calculated by use of this program can be found in Appendix II.

FIGURE XIX

LOGIC FLOW OF COMPUTER PROGRAM

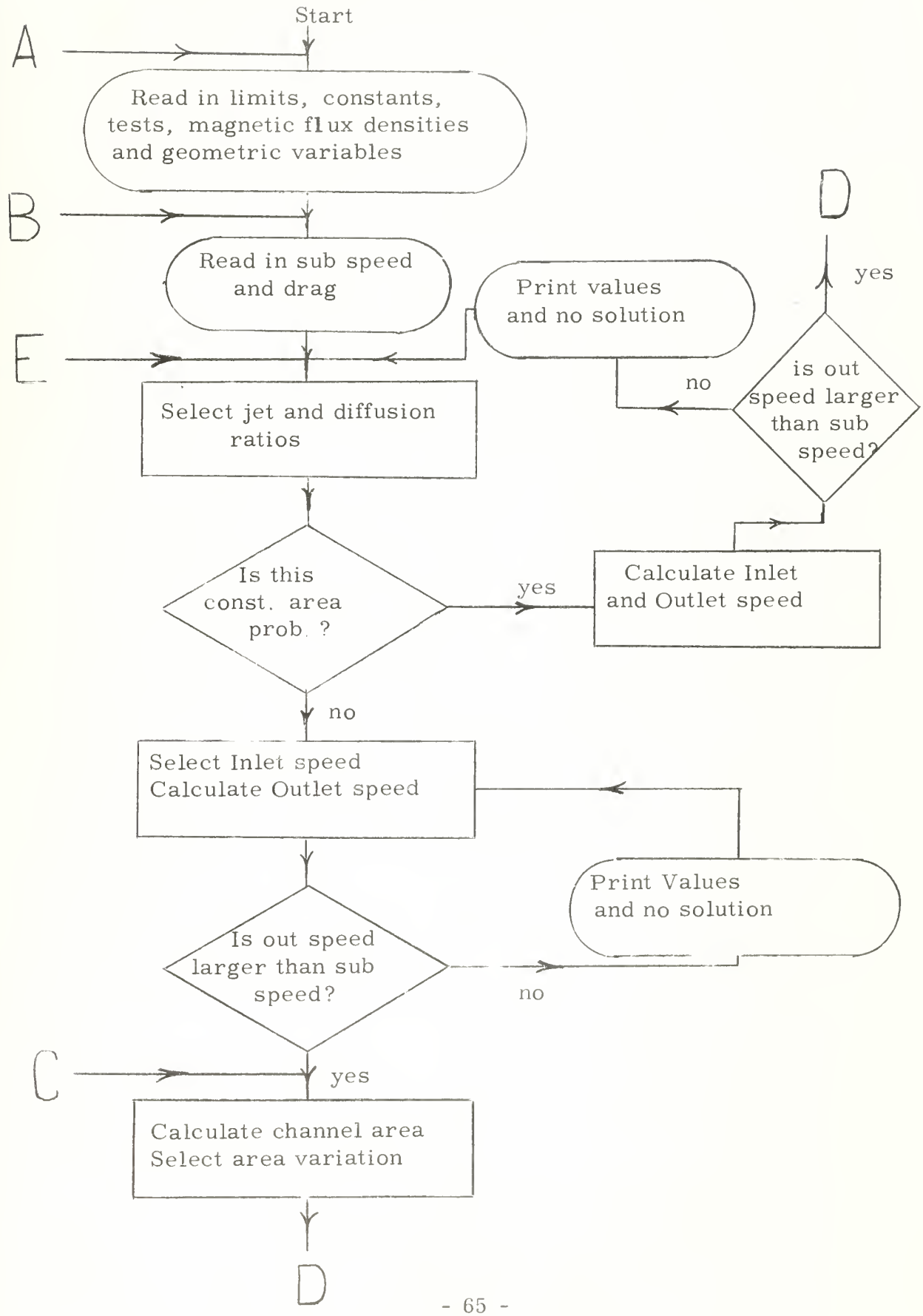

FIGURE XIX (Cont.)

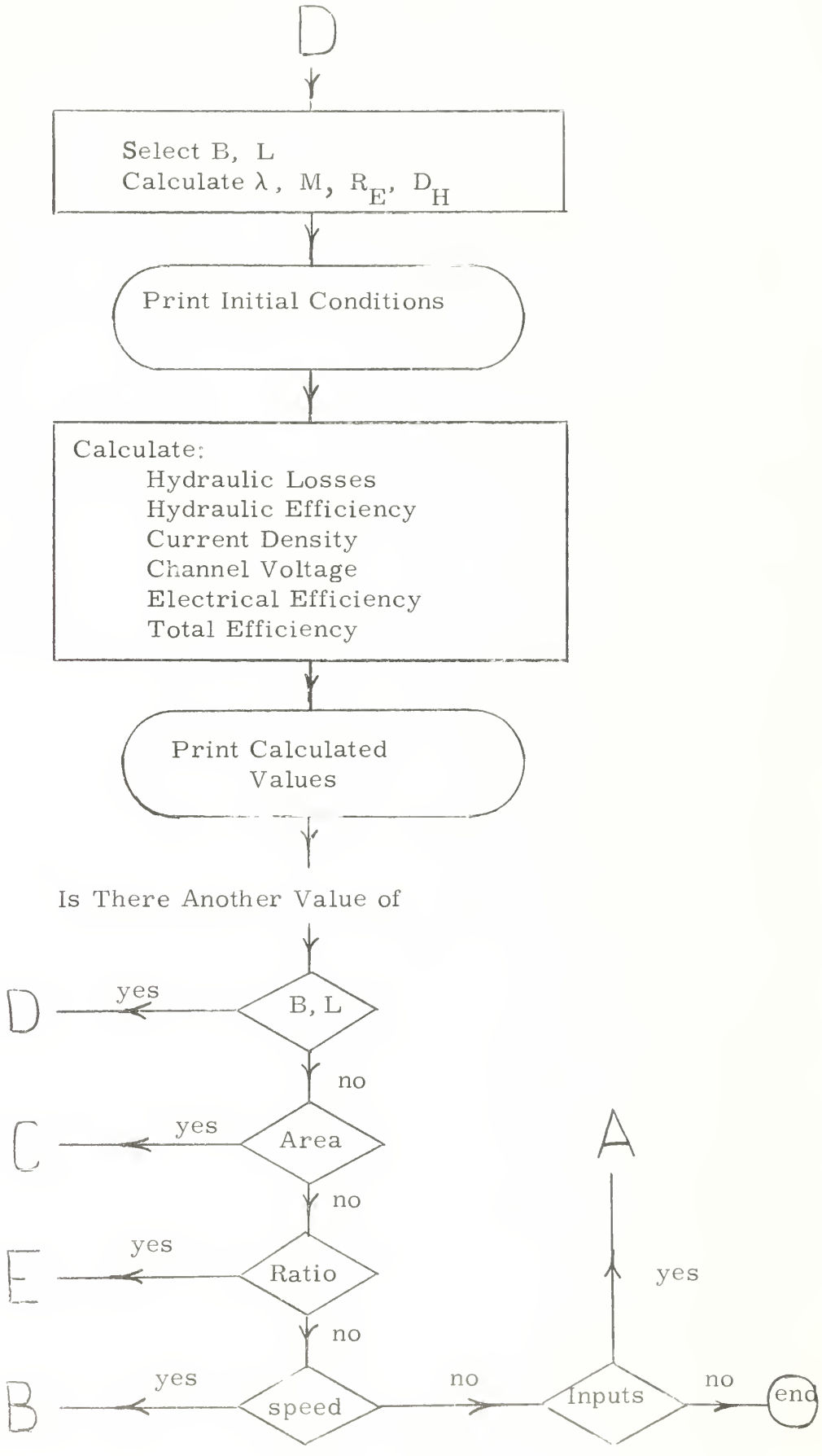

APPENDIX II

DATA AS CALCULATED USING IBM 7090 DIGITAL COMPUTER FOR FIGURES OF CHAPTER V

Data for Figure XIII

Submarine Speed 30 KTS = 50.65 FT/SEC

Diffuser Ratio = 1.05

Magnetic Flux Density = 20 WEBERS/M^2

Inlet Speed = 50.6 FT/SEC

Jet Ratio	Channel Area	Total Effic.	Channel Length	Hydraulic Efficiency	Electrical Efficiency
	(FT^2)		(FT)		
1.1	427	.745	50	.785	.950
		.710	75	.738	.962
		.682	100	.705	.968
		.650	125	.670	.971
1.22	125	.688	50	.785	.877
		.693	75	.760	.912
		.685	100	.737	.930
		.673	125	.715	.942
1.35	70	.570	50	.730	.780
		.600	75	.715	.840
		.605	100	.692	.875
		.605	125	.676	.895
1.500	66	.500	50	.700	.715
		.540	75	.691	.782
		.560	100	.679	.824
		.570	125	.671	.851
2.33	16	.230	50	.560	.412
		.280	75	.555	.505
		.315	100	.550	.573
		.340	125	.545	.625

Data For Figures XIV and XV

Magnetic Flux Density = 20 WEBER/M^2

Channel Length = 50 FEET

Submarine Speed = 5 KTS = 8.44 FT/SEC

Inlet Speed = 8.72 FT/SEC

Diffuser Ratio	Area	Hydraulic Efficiency	Electrical Efficiency	Total Effic.	Jet Ratio	Outlet Inlet Ratio
1.05	74.63	.6365	.9515	.6057	1.35	1.285
	49.76	.6413	.9294	.5961	1.50	1.430
1.10	99.30	.640	.9570	.612	1.35	1.228
	61.43	.643	.9370	.6026	1.50	1.363
1.15	135.5	.618	.963	.596	1.35	1.174
	76.74	.6392	.9441	.6035	1.50	1.304
1.20	195.0	.580	.970	.562	1.35	1.124
	98.0	.640	.950	.608	1.50	1.250
1.25	330.0	.550	.976	.547	1.35	1.080
	127.0	.621	.958	.595	1.50	1.200

Data For Figures XIV and XV

Magnetic Flux Density = 20 WEBER/M^2

Channel Length = 50 FEET

Submarine Speed = 20 KTS = 33.76 FT/SEC

Inlet Speed = 34.87 FT/SEC

Diffuser Ratio	Area	Hydraulic Efficiency	Electrical Efficiency	Total Effic.	Jet Ratio	Outlet Inlet Ratio
1.05	62.59	.6514	.8338	.5432	1.35	1.285
	41.73	.6538	.7705	.5038	1.50	1.430
1.10	82.20	.650	.855	.555	1.35	1.228
	51.52	.6556	.7911	.5187	1.50	1.363
1.15	106.0	.620	.872	.5400	1.35	1.174
	64.3	.6516	.8114	.5288	1.50	1.304
1.20	167.52	.5969	.9019	.5385	1.35	1.124
	80.5	.643	.831	.535	1.50	1.250
1.25	272.0	.550	.916	.503	1.35	1.080
	106.3	.610	.850	.518	1.50	1.200

Data For Figures XIV and XV

Magnetic Flux Density = 20 WEBER/M^2

Channel Length = 50 FEET

Submarine Speed = 30 KTS = 50.65 FT/SEC

Inlet Speed = 52.30 FT/SEC

Diffuser Ratio	Area	U IN	Hydraulic Efficiency	Electrical Efficiency	Total Effic.	Jet Ratio	Outlet Inlet Ratio
1.05	64.62	52.30	.6537	.7705	.5038	1.350	1.285
	43.08	52.30	.6558	.6919	.4538	1.500	1.430
1.10	85.50	52.30	.6500	.7960	.517	1.350	1.228
	53.19	52.30	.6575	.7169	.4715	1.500	1.363
1.15	118.0	52.30	.615	.824	.507	1.350	1.174
	66.44	52.30	.6535	.755	.4850	1.500	1.304
1.20	168.5	52.30	.567	.853	.483	1.350	1.124
	83.0	52.30	.649	.776	.503	1.500	1.250
1.25	283	52.30	.507	.888	.450	1.350	1.080
	109.3	52.30	.634	.792	.501	1.500	1.200

Data For Figures XIV and XV

Magnetic Flux Density = 20 WEBER/M^2

Channel Length = 50 FEET

Submarine Speed = 50 KTS = 84.39 FT/SEC

Inlet Speed = 87.16 FT/SEC

Diffuser Ratio	Area	Hydraulic Efficiency	Electrical Efficiency	Total Effic.	Jet Ratio	Outlet Inlet Ratio
1.05	59.07	.6543	.6684	.4374	1.35	1.285
	39.38	.6563	.5741	.3768	1.50	1.430
1.10	78.0	.637	.713	.455	1.35	1.228
	48.62	.6580	.6033	.3970	1.50	1.363
1.15	102.0	.632	.738	.467	1.35	1.174
	60.73	.6539	.6333	.4142	1.50	1.304
1.20	154.5	.568	.776	.441	1.35	1.124
	77.1	.645	.665	.429	1.50	1.250
1.25	258.0	.520	.792	.411	1.35	1.080
	100.0	.632	.698	.443	1.50	1.200

Data For Figures XIV and XV

Magnetic Flux Density = 20 WEBER/M^2

Channel Length = 50 FEET

Submarine Speed = 100 KTS = 168.79 FT/SEC

Inlet Speed = 174.83 FT/SEC

Diffuser Ratio	Area	Hydraulic Efficiency	Electrical Efficiency	Total Effic.	Jet Ratio	Outlet Inlet Ratio
1.05	54.45	.6556	.5025	.3295	1.35	1.285
	36.30	.6574	.4031	.2650	1.50	1.430
1.10	72.20	.645	.543	.350	1.35	1.228
	44.82	.6590	.4323	.2850	1.50	1.363
1.15	98.30	.626	.587	.368	1.35	1.174
	55.98	.6549	.4638	.3038	1.50	1.304
1.20	142.2	.568	.635	.361	1.35	1.124
	71.2	.654	.498	.326	1.50	1.250
1.25	235.0	.480	.700	.336	1.35	1.080
	93.0	.632	.536	.339	1.50	1.200

Data For Figures XVI, XVII, And XVIII

Channel Length = 50 FT

Diffuser Ratio = 1.05

Case I Channel Area = 50 FT^2

Jet Ratio = 1.680

Sub Speed (KTS)	Inlet Speed (FT/S)	Current Density Amps/M^2)	Channel Voltage (Volts)	Mag. Flux Density (Webers/M^2)	E_H	E_{EL}	E_{Total}
5	7.32	57	54	5	.808	.426	.344
		29	62	10	.808	.747	.560
		19	79	15	.808	.869	.696
		14	100	20	.808	.921	.735
20	26.81	764	497	5	.888	.169	.150
		382	375	10	.888	.460	.399
		255	390	15	.888	.655	.575
		191	440	20	.888	.765	.680
30	40.86	1772	1087	5	.876	.118	.103
		886	736	10	.876	.339	.306
		590	705	15	.876	.535	.479
		443	753	20	.876	.670	.597
50	65.11	4492	2634	5	.882	.077	.068
		2246	1624	10	.882	.252	.222
		1497	1423	15	.882	.431	.380
		1123	1425	20	.882	.574	.505
100	125.03	16527	9334	5	.852	.0421	.036
		8264	5256	10	.852	.149	.127
		5509	3806	20	.852	.413	.352

Data For Figures XVI, XVII, And XVIII

Channel Length = 50 FT

Diffuser Ratio = 1.05

Case II Channel Area = 75 FT^2

Jet Ratio = 1.490

Sub Speed (KTS)	Inlet Speed (FT/S)	Current Density (Amps/M^2)	Channel Voltage (Volts)	Mag. Flux Density (Webers/M^2)	E_H	E_{EL}	E_{Total}
5	7.15	36	51	5	.881	.536	.472
		18	67	10	.881	.821	.717
		12	90	15	.881	.911	.793
		9	116	20	.881	.948	.822
20	26.20	478	417	5	.895	.241	.216
		239	360	10	.895	.560	.501
		159	408	15	.895	.741	.663
		119	482	20	.895	.836	.749
30	39.92	1108	887	5	.876	.173	.155
		554	674	10	.876	.456	.408
		369	705	15	.876	.653	.584
		277	797	20	.876	.770	.688
50	63.62	2808	2105	5	.895	.116	.104
		1404	1419	10	.895	.345	.309
		936	1354	15	.895	.542	.485
		702	1444	20	.895	.678	.607
100	122.16	10325	7310	5	.875	.064	.056
		5162	4360	10	.875	.215	.188
		3442	3690	15	.875	.382	.334
		2581	3590	20	.875	.524	.458

Data For Figures XVI, XVII, And XVIII

Channel Length = 50 FT

Diffuser Ratio = 1.05

Case III Channel Area = 100 FT^2

Jet Ratio = 1.37

Sub Speed (KTS)	Inlet Speed (FT/S)	Current Density ($Amps/M^2$)	Channel Voltage (Volts)	Mag. Flux Density ($Webers/M^2$)	E_H	E_{EL}	E_{Total}
5	7.19	25	52	5	.901	.622	.566
		12	74	10	.901	.867	.781
		8	103	15	.901	.936	.839
		6	134	20	.901	.963	.858
20	26.33	338	379	5	.890	.312	.284
		169	367	10	.890	.644	.586
		112	441	15	.890	.803	.731
		84	538	20	.890	.879	.800
30	40.13	782	785	5	.910	.229	.208
		391	663	10	.910	.543	.494
		260	742	15	.910	.728	.661
		196	872	20	.910	.826	.751

APPENDIX III

BIBLIOGRAPHY

1. PHILLIPS, O.M., "The Prospects for Magnetohydrodynamic Ship Propulsion", Journal of Ship Research, March 1962, pp. 43 - 51;

2. FRIAUF, J.B., "Electromagnetic Ship Propulsion", Journal of the American Society of Naval Engineers, February 1961, Vol. 73, No. 1;

3. HARTMANN, J. and LAZARUS, F., "Hg-Dynamics II", Kgl. Danske Videnskab. Selskab, Mat.-fys., Medd. 15, 7, 1937;

4. MURGATROYD, W., "Experiments on Magneto-Hydrodynamic Channel Flow", Phil. Mag., Vol. 44, 1953, pp. 1348-1354;

5. BROUILLETTE, E.C. and LYKOUDIS, P.S., "Measurements of Skin Friction for Turbulent Magnetofluid-mechanic Channel Flow", Purdue Research Foundation, Research Project No. 3093, August 1962;

6. CUSAK, N., The Electrical and Magnetic Properties of Solids, John Wiley, New York, N. Y., 1958, Chapter 16;

7. HAKE, R., Bulletin American Physics Society, Series 2, Vol. 6, 1961, pp. 425;

8. KUNZLER, J.E., Bulletin American Physics Society, Series 2, Vol. 6, 1961, pp. 278;

9. KUNZLER, J.E., et al, "Superconductivity in Nb_3Sn at High Current Density in a Magnetic Field of 88 Kilogauss", Physical Review Letters, February 1961;

10. GELLER, S., Acta Crypt., Vol. 9, 1956, pp. 885;

11. WERNICK, J.H., et al, "Evidence for a Critical Magnetic Field in Excess of 500 Kilogauss in the Superconducting V-Ga System", High Magnetic Fields, MIT Press and John Wiley, New York N.Y., 1962, pp. 609-614;

12. HARRIS, L.P., Hydromagnetic Channel Flows, MIT Press and John Wiley, New York N. Y., 1960;

13. MILLIKAN, C.B., "Turbulent Flows in Channels and Circular Tubes", Proc. Fifth International Congress for Applied Mechanics, John Wiley, New York, N. Y., 1939, pp. 390;

14. SCHLICHTING, H., Boundary Layer Theory, Pergamon Press, New York, N. Y., 1955, pp. 405;

15. SHERCLIFF, J.A., "Steady Motion of Conducting Fluids in Pipes Under Transverse Magnetic Fields", Proc. Camb. Phil. Soc., 1953, pp. 136-144;

16. NIKURADSE, J., " Untersuchung uber die Geschwindigkeitsverteilung in Turbulenten Stromungen", VDI-Forschungsheft 281, Berlin, 1926;

17. HOAGLAND, L.C., Fully Developed Turbulent Flow in Straight Rectangular Ducts, M.I.T. Thesis, 1960;

18. LAUFER, J., "Investigation of Turbulent Flow in a Two-Dimensional Channel", NACA Report 1053, Washington, 1951;

19. SUTTON, B.W., "The Theory of Magnetohydrodynamic Power Generators", General Electric Technical Information Series R62SD990, December, 1962, pp. 88 - 96;

20. FANO, et al, Electromagnetic Fields, Energy, and Forces, John Wiley, New York, N. Y., 1960, pp. 481;

21. ARENTZEN, E.S. and MANDEL, P., "Naval Architectural Aspects of Submarine Design", Transactions of the Society of Naval Architects and Marine Engineers, 1960, pp. 50;

22. Ibid., pp. 10;

23. DTMB Report 806, 1954, pp. 40;

24. HOERNER, S.F., Fluid Dynamic Drag, Published by author, pp. 9-9;

25. PRIOR, B.J. and HALL, C.N., "Subsonic Wind Tunnel Tests of Various Forms of Air Intakes Installed in a Fighter Type Aircraft", ARC Technical Report No. 3134, Her Majesty's Stationary Office, London, 1960, pp. 31;

26. HULM, J.K., et al., "A High Field Niobium Zirconium Superconducting Solenoid", High Magnetic Fields, MIT Press and John Wiley, New York, N. Y., 1962, pp. 332-340;

27. STEKLY, Z.J.J., Magnetic Energy Storage Using Superconducting Coils, from Avco-Everett Research Laboratory, Everett, Mass., Unpublished;

28. LEVY, R.H., ARS Journal, Vol. 32, May 1961, pp. 787.